AN ABSTRACT OF THE THESIS OF

Jon Michael Bosley for the degree of Master of Science in Geography presented on December 1, 2006.

Title: Mapping Vegetation Density and Water Inundation in a Recovering Wetland: The Mesopotamian Marshlands

Abstract approved:

_____

Anne W. Nolin

Once considered the largest wetland in Central Asia, the Mesopotamian Marshlands of Southeastern Iraq have nearly disappeared. Various hydrological projects by the Iraqi government and dam construction in the region have nearly destroyed these once rich freshwater wetlands by over 90%. With the launching of Operation Iraqi Freedom recent attempts at restoration have been undertaken. To assess these changes and determine the success of restoration attempts this study is using 275-m multiangular MISR imagery to measure vegetation densities and water inundation patterns. By implementing a mapping method called spectral linear unmixing, fractional estimates of vegetation and water have been determined for six images from 2000-2005. Three subsets of the MISR imagery are compared: multispectral + multiangular, multispectral bands only, and multiangular bands only. Spectral linear unmixing, from all three subsets show a change in vegetation coverage from an average of 4490 km^2 in 2000, to 9584 km^2 in 2005 representing an increase of 114%. Results for water inundation also indicate an

average increase of 109% from 3814 km^2 in 2000 to 7986 km^2 in 2005. To validate the MISR estimates, I compared these results with fractional estimates of vegetation and water derived from high spatial resolution 2-m QuickBird imagery based on data from 2002 and 2005. Each MISR image is rescaled to the 2-m spatial resolution of QuickBird so that a pixel-by-pixel comparison can be made. The validation results for 2002 and 2005 shows the multispectral + multiangular MISR approach identifies 28% of the water that QuickBird detects. Separately, multispectral and multiangular subsets were only able to detect 11% each. When examining vegetation coverage the multispectral subset is able to detect 69% whereas the multispectral + multiangular, and multiangular subsets detect 61% and 21%, respectively. Results presented in this paper are encouraging and suggest that the Mesopotamian Marshlands is recovering as vegetation is establishing and water is once again present. Interseasonal and interannual images may improve results and be more representative of the region.

Mapping Vegetation Density and Water Inundation in a Recovering Wetland: The Mesopotamian Marshlands

by:

Jon Michael Bosley

A THESIS

submitted to

Oregon State University

in partial fulfillment of
the requirements for the
degree of

Master of Science

Presented December 1, 2006
Commencement June 2007

Master of Science thesis of Jon Michael Bosley presented on 01 December 2006.

APPROVED:

_____

Major Professor, representing Geography

_____

Chair of the Department of Geosciences

_____

Dean of the Graduate School

I understand that my thesis will become part of the permanent collection of Oregon State University libraries. My signature below authorizes release of my thesis to any reader upon request.

_____

Jon Michael Bosley, Author

ACKNOWLEDGEMENTS

I would like to sincerely thank my academic advisor Anne Nolin for all her help and inspiration. Over the last few years, Anne has put in a great deal of time and energy to ensure that my transition into a graduate student was easy and that success was inevitable. I would also like to thank my committee members for their time, effort and patience: A Jon Kimerling, Mary Santelmann, and Rob Harris who is serving as my graduate school representative.

I would also like to thank the *Aquaculture Collaborative Research Support Program for providing me with funds that have been used in the purchase of satellite imagery used in this research. Continued support from my friends and family is also greatly appreciated.

Lastly I would like to thank the West Virginia University McNair Scholars program for providing me with the strength and support to take on the challenges of an advanced degree. The McNair Scholars program also provided me with a brilliant mentor and friend in Tim Warner who has been very supportive over the years.

*The contents of this document do not represent an official position or policy of the United States Agency for International Development (USAID). Mention of trade names or commercial products in the reports does not constitute endorsement or recommendation for use on the part of USAID or the Pond Dynamics/Aquaculture Collaborative Research Support Program

TABLE OF CONTENTS

LIST OF FIGURES

Figure Page

LIST OF FIGURES (Continued)

LIST OF FIGURES (Continued)

Figure Page

LIST OF FIGURES (Continued)

Figure Page

LIST OF TABLES

Mapping Vegetation Density and Water Inundation in a Recovering Wetland:
The Mesopotamian Marshlands

Introduction

The Mesopotamian Marshlands of Southeastern Iraq represents one of the largest wetland ecosystems in all of Asia (Thesiger, 1957; Scott 1995; Partow, 2001) and is formed by the confluence of the Tigris and Euphrates Rives. This ecoregion has historically served as home to an abundance of birds, fish, mammals, and ancient communities including the Sumerian culture, for over 5,000 years. Residents of the marshes, the Ma'dan, commonly live on "floating islands" and are highly dependent on sustainable fishing and farming as a way of survival.

During the last two decades, hydrological programs such as Iraqi government drainage and Turkish dam construction in the headwaters of the Tigris and Euphrates Rivers (Gruen, 2002) have nearly destroyed these once-rich freshwater wetlands (Maltby, 1994). The wetlands are fed by spring snowmelt from the Taurus mountains of Turkey and the Zagros mountains of Iran. The biogeochemical cycling of this extensive wetland region, when in its natural state, plays an important role in improving degraded water quality in the lower Tigris and Euphrates basin (Partow, 2001). The Mesopotamian Marshlands, once covering an area over 20,000 km^2, has been reduced by over 90% (Partow, 2001).

In the spring of 2003, the military invasion of Iraq led to demolition of a number of water diversion structures in the marshlands. Water again has been flowing into these wetlands, the inundated area has increased, and vegetation appears to be regrowing

(Mertes, 2004). However, with the ongoing political strife and military dangers in the region, there are limited fieldwork opportunities to monitor these significant changes.

Satellite remote sensing offers the capability of tracking land-cover change such as vegetation regrowth and water inundation patterns. Previous work has shown that multi-spectral and multi-angular remote sensing approaches can successfully track fraction canopy attributes in transitional zones (Chopping et al., 2003), wetland vegetation and inundation (Hess et al., 2003), and woody shrub abundances over desert grasslands while accounting for upper canopy and background influences (Chopping et al., 2006).

The overarching goal of this study is to map the re-growth of vegetation in the marshlands. Towards this end, specific objectives include:

1. Demonstrating the utility of a combined multiangular-multispectral-approach for mapping wetland recovery;
2. Characterizing the spatial and temporal changes in vegetation re-growth; and
3. Relating vegetation re-growth to water inundation patterns.

Background and Previous Work

Recent Changes in Inundation of the Mesopotamian Marshlands

Beginning in the early 1970s and continuing into the 1990s a variety of factors have seriously altered the marshlands from their original, pristine condition. The first series of major events began in the early 1970s when dam construction in the headwaters of the Tigris and Euphrates Rivers (major sources for the marshes) began to alter the annual pattern of streamflow, reducing spring snowmelt floods and mitigating summer low-flow. In the summer of 1991 the Iraqi Government began construction on massive hydrological projects to control and regulate the marshland water drainage. According to the Iraqi Government, these programs were engineered to reduce salinization problems on millions of hectares of agricultural land, to retrieve new land for food production, and to increase the amount of water for irrigation (Scott, 1995). Partly as a result of these hydrological projects, the once-rich freshwater wetlands, home to fish, mammals, birds, and almost a half a million people (known as the "Marsh Arabs"), have been destroyed. This area, once covering over 20,000 km^2 has been reduced by over 90% (Partow, 2001).

During the mid-to-late 1980s (Scott, 1995) an increase in water salinity began to emerge as a major threat to the marshland region, most notably in the Hawr al Hammar. From the early 1980s until the early 1990s the salinity in the Shatt al Arab, at Qarmat Ali, increased from 0.5 parts per thousand (ppt) to over 2.0 ppt (Scott, 1995). The estuarine systems formed by these marshes provide a habitat and spawning ground to several

marine fish of economic importance; i.e. the saboor (*Hilsa hilsa),* bunni (*Barbus sharpeyi)*, khatan (*Barbus xanthopterus)*, himri (*Barbus luteus)*, and the shaboot (*Barbus grypus)* (Scott, 1995).

In addition to increased water salinity and government-regulated hydrological projects, another destructive practice soon emerged: dam construction in the headwaters of the Tigris and Euphrates rivers. During the late 1970s through the 1980s Turkey developed plans for a $32 billion project called the Southeastern Anatolia Project (Güneydoğu Anadolu Projesi-GAP), which will consist of 22 dams of which 12 are complete and 19 hydro-electrical power plants of which 6 are complete on the Tigris and Euphrates Rivers (Gruen, 2000; Mann, 2003). This project will regulate over 28% of Turkey's water potential (Embassy, 2006). After GAP is complete, the dam system will irrigate around 17,000 square kilometers of land, generate 27 billion Kwhs of electric energy and increase the total arable land by 50%.

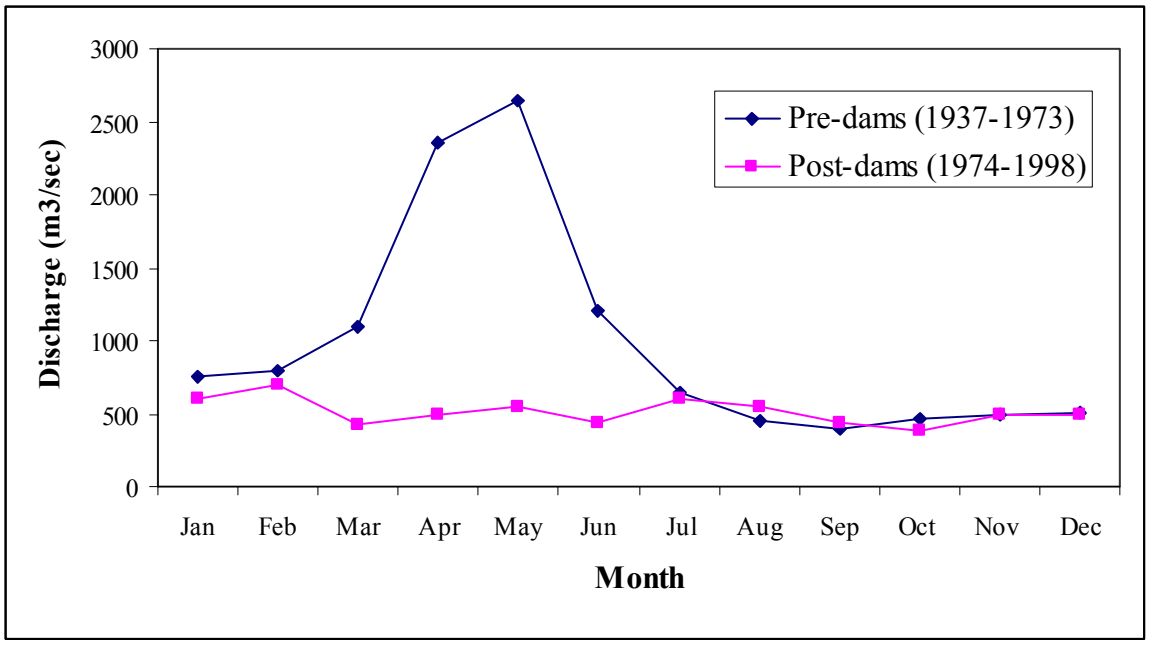

Figure 1. Average monthly discharge of the Euphrates River at Hit Husabi Iraq

Figure 1 shows the discharge of the Euphrates River at Hit-Husabi (central Iraq, west of Baghdad) during two time periods: pre-dam construction (1938-1973) and post dam-construction (1974-1998) UNEP (2001) and Altinbilek (2004). The effects of dam construction on the Euphrates can be illustrated in the month of May. During the "post-dam" construction era, the peak water flow in May decreased from ~2600 m^3/s to ~800 m^3/s. In addition, the overall minimum flow increased from 272 to 575 m^3/s. The dams have eliminated the seasonal floods on which the marshes depend for flushing excess salinity and freshening the wetlands.

As of there are over 32 major dams on the Tigris and Euphrates and with the addition of GAP, this number will greatly increase (Partow, 2001). Turkey and Syria

continue to implement plans to dam the rivers for economic benefits including hydro-electrical power, irrigation and consumption.

Since the start of the American-led military effort Operation Iraqi Freedom in 2003, there have been profound impacts on both the country and the marshlands. The Mesopotamian Marshlands have been re-flooded and limited attempts at restoration have begun. With improved water quality, recovery of soils, and presence of native species in certain regions, Richardson et al. (2005) assert that the region has reasonable potential for ecological restoration.

To achieve this potential a comprehensive monitoring program is needed. However with limited fieldwork opportunities and resources satellite remote sensing offers the potential for multi-temporal mapping of the inundated area and vegetation establishment. Studies have shown that using multiangular and multispectral remote sensing data, vegetation density can be successfully mapped (Gobron et al., 2002; Widlowski et al., 2001; Pinty et al., 2002; Nolin, 2004). Additionally, multiangular data can be used to infer vegetation structure and density whereas multispectral reflectance data provides information on vegetation health and biomass.

Description of the Study Area

Formation of the Marshes

A distinct characteristic of the lower Tigris and Euphrates River Basin is the extremely low relief of its alluvial plains. The lack of topography allows both rivers to deviate from a straight, single channel and divide into distributaries filtering into a vast inland delta inundating the area and laying the foundation for marshland formation (Partow, 2001). Water sources for the Tigris River first originate in the high mountains of Eastern Turkey, as a result of snowmelt, near Diyarbakir, and Batman-Su. Near the town of Ceffan these two sources join together to unite the Tigris, which then flows around 100 km more before it reaches the Syrian border (Kliot 1994). Likewise, the two main water sources for the Euphrates, the Furat-Su and the Murat-Su, originate in the mountains of Eastern Turkey. The Furat-Su flows along a course of 450 km to meet up with the Murat-Su, which then converges to form the basis of the Euphrates River. Snowmelt from the Taurus and Zagros mountains also provides both the Furat-Su and Murat-Su with its precipitation (Kliot, 1994)

In addition to the lack of topography, another influencing factor in the marshland formation is that the marshland plains, associated with the Tigris and Euphrates, become very narrow towards the Persian Gulf. As a result the rivers tend to overflow into the plains. This overflow forces the rivers to deposit their sediment loads further inland creating a double delta, composed of a continental marshland complex and a marine estuary (Partow, 2001).

Major Marshland Units

The Mesopotamian Marshlands are comprised of three major marshes (Figure 2): Hawr al Hammar, al-Qurnah (also known as the Central Marsh) and Hawr al Hawizeh.

Situated almost entirely south of the Euphrates, Hawr al Hammar extends roughly from Al-Nasiriyah in the west to al-Basrah in the east. Dominating the marshes by extending a length of 120 km and a width of 25 km (at its maximum), al Hammar Lake is considered to be the largest body of water in the lower Euphrates. The lake's maximum depth ranges from a low of 1.8 meters to a high of 3 meters (Maltby, 1994; Scott, 1995; Partow, 2001). In its natural state, Hawr al Hammar covered an area of 2800 km^2. During periods of heavy rain and inundation this can increase to over 4500 km^2 (Partow, 2001).

Located immediately upstream of the confluence of the Tigris and the Euphrates Rivers, al Qurnah is bounded by the Tigris River to the east and the Euphrates River in the south. This area is roughly triangulated between Al Nasiriyah, Qalat Saleh and al Qurnah. In its natural state the size of al Qurnah ranged from 3000 km^2 to over 4000 km^2 during periods of inundation (Partow, 2001). Two of the more prominent lakes in the region are al Zikri and Hawr Umm al Binni, which are approximately 3 meters deep (Thesiger, 1957; Scott, 1995; Partow, 2001).

Hawr al Hawizeh is bordered by Iran to the east and the Tigris River to the west. Known as Hawr al-Azim in Iran, al Hawizeh is largely fed by two main water sources departing from the Tigris River. In its natural state, al Hawizeh can extend 80 km from north to south and 30 km from east to west, accounting for an average area of over 3000

km^2 (Partow, 2001). The marsh is composed of a permanent portion, which contains extensive Phragmites reed beds, and a seasonal portion which contains Common Reed (Scott, 1995). During periods of heavy rains and inundation, al Hawizeh would increase to an area of over 5000 km^2 (Partow, 2001). With depths over 6 meters, large permanent lakes can be found in the northern part of the region (Maltby, 1994; Partow, 2001).

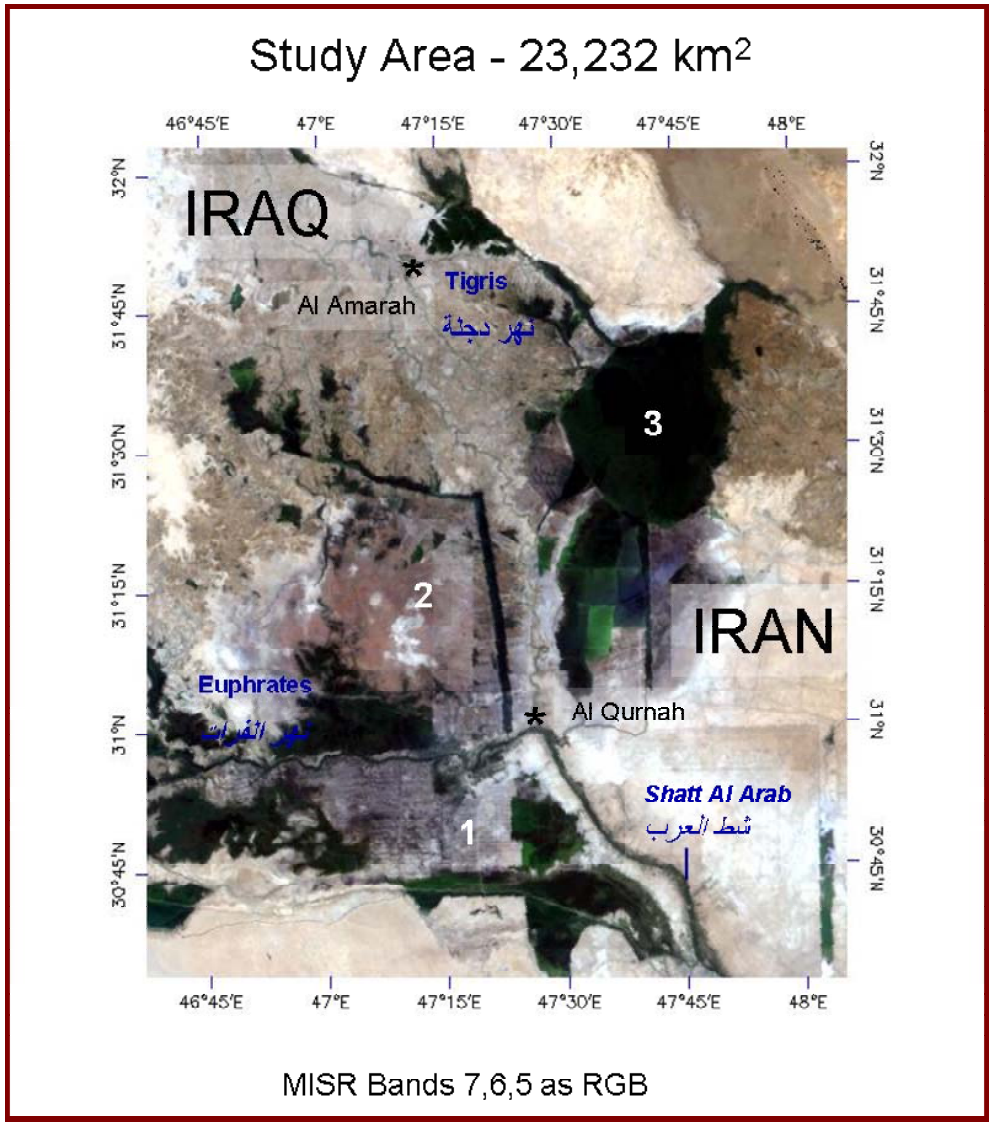

Figure 2. Locations of the Mesopotamian Marshlands shown in true color; 1) Hawr al Hammar, 2) al Qurnah and 3) Hawr al Hawizeh

Flora and Fauna of the Marshes

It is estimated that when in their natural state, the Mesopotamian Marshlands are home to several million wintering water-fowl (two thirds of western Asia's total). Partow, (2001) estimates that there are over 134 bird species permanently residing in the marshes (11 of which are globally threatened). The marshes also support almost the entire global population of the basrah reed warbler (*Acrocephalus griseldis*) and the Iraq babbler (*Turdoides altirostris*) (Maltby, 1994; Scott 1995). *Table 1* (reprinted from Partow, 2001), lists species of the marshes that are considered to be highly threatened:

Table 1. Threatened and endangered species that reside in the Mesopotamian Marshlands.

Common Name	Scientific Name
Birds	
Iraq Babbler (endemic)	*Turdoides altirostris*
Basrah Reed Warbler (endemic)	*Acrocephalus griseldis*
African Darter (sub-species)	*Anhinga rufa chantrei*
Dalmatian Pelican	*Pelecanus crispus*
Goliath Heron	*Ardea goaliath*
Imperial Eagle	*Aquila heliaca*
Marbled Teal	*Marmaronette angustirostris*
Pygmy Cormorant	*Phalacrocorax pyhmaeus*
Sacred Ibis	*Threskiornis aethiopicus*
Slender-billed Curlew	*Numenius tenuirostris*
White-Tailed Eagle	*Haliaeetus albicilla*
Mammals	
Smooth-coated Otter	*Lutra perspeicillata*
Smooth-coated Otter (sub-species)	*maxwelli*
Grey Wolf	*Canis lupus*
Long-fingered Bat	*Myotis capaccinii*

Bandicoot Rat	*Erthyronesokia bunnii*
Harrison's Gerbil	*Gerbillus mesopotamicu*
Amphibians and Reptiles	
Soft-Shelled Turtle	Soft-Shelled Turtle
Desert Monitor	Desert Monitor
Fish	
Gunther (endemic species)	Gunther (endemic species)
Invertebrates	
Dragonfly	Dragonfly

In addition to the threatened species listed in *Table 1,* several fish known to spawn in the marshes include the endemic giant catfish (*Silurus glanis and S. Triostegus*), the hilsa shad (*Tenualosa ilisha*), and a pomphret (*Pampus argenteus*) (Partow, 2001; Scott, 1995).

The marshland region is dominated by common reed (*Phragmites australis*), narrow-leafed cattail (*Typha angustifolia*), and papyrus (*Cyperus papyrus*). Common reed dominates the more permanent areas of marshes, while the narrow-leafed cattail dominates the more seasonally wet areas (Thesiger, 1957; Scott, 1995). In Table 2, (compiled from data collected by Scott, 1995), species commonly (surface and subsurface) found in the marshes are listed:

Table 2. Several common types of vegetation (submerged and surface) found in the marshland region (after Scott, 1995).

Common Name	Scientific Name
Submerged Aquatic Vegetation (found in deep permanent lakes)	
Hornwort	*Ceratophyllum demersum*
Eel Grass	*Vallisneria spiralis*
Pondweed	*Potamogeton lucens* *Potamogeton pectinatus*
Water Milfoil	*Myriophyllum spiralis*
Stonewort	*Chara spiralis*
Naiads	*Najas marina* *Najas armata*
Water Fern	*Salvinia spiralis*
Surface Vegetation (found on smaller lakes and backwaters)	
Water-lilies	*Nymphoides peltata* *Nymphoides indica* *Nymphaea caerulea* *Nuphar spiralis*
Water Soldier	*Pistia stratitoes*
Duckweed	*Lemna gibba*

Additionally the marshes are home to a settlement of people, the Ma'dan, who are commonly referred to as the "Marsh Arabs." During the 1980s it was estimated that the total population of the Marsh Arabs was between 350,000 and 500,000. Descendants of the Sumerians and Babylonians, the Marsh Arabs have unique lifestyles that are firmly rooted in the marshes. Settlements are commonly found on floating islands, which are reinforced with reeds and mud, or along the edges of the marshes (Partow, 2001).

If drainage of the marshes were to continue, the effects on the population of flora, fauna and the indigenous people could be devastating. In addition to the threatened species mentioned earlier, Scott and Evans (1994), have determined that the *Lutra*

perspicillata maxwelli and *Erythronesokia bunnii,* would become globally extinct, the *Anhinga rufa* and *Threskiornis aethiopicus* would become extinct in the Middle East, and the *Phalacrocorax pygmaeus* and *Ardea goliath* would become extinct in Iraq.

Remote Sensing Methods for Mapping Inundation and Vegetation

During the past 20 years new techniques using multispectral imagery to map and characterize inundated floodplains (e.g. Mertes, 1997; Smith 1998), and vegetation (e.g. Jones and Muthuri, 1985) have emerged.

Mertes (1997), look at the importance of the perirheic zone on inundated floodplains (on the Missouri, Mississippi, Amazon, Ob'-Irtysh, Taquari, and Altamaha ed), and determined that the perirheic zones may influence geomorphology, biogeochemistry, vegetation cover, and productivity of the floodplains. Jones and Muthuri (1985) examined papyrus canopy structure in Kenya and Rwanda and determined that the upper two meters of the canopy intercepts over 90% of photosynthetic active radiation. Additionally, root structure is an important influencing factor in the growth of papyrus, a common reed of the Mesopotamian Marshlands.

Vanderbilt et al. (2002) used multispectral/multiangular POLarization and Directionality of the Earth's Reflectance (POLDER) data (from central Saskatchewan Canada) to discriminate between inundated and non-inundated community types based on properties of sun glint (surface water characteristics of angular reflectance). By using properties of sun glint Vanderbilt et al. were successful in discriminating three cover types (emergent inundated vegetation, open water and non-inundated vegetation) and concluded that this new approach is promising in mapping seasonal and biannual

inundation. However, in order to correctly classify wetlands using glitter properties, ground references must be known.

Nolin (2004) examined forest cover density in north central Colorado using Multiangle Imaging SpectroRadiomer (MISR) imagery and determined that there is a positive correlation between forest cover density and the pattern of multiangular reflectance. This paper suggests that the angular pattern of reflectance provides information on forest density.

By testing multiangular imagery acquired from the DuncanTech camera with detailed ground observations, Chopping et al. (2003) were able to track fractional canopy attributes in several transitional zones in New Mexico. Chopping et al. determined that by inverting the Simple Geometric Model (SGM) of the bi-directional reflectance distribution function (BRDF) structural canopy attributes (density, width, and height) could be derived. The SGM is intended for the purpose of inversion against multiangular data. When adjusted to multiangular data, the SGM provides structural attributes not available from nadir only imagery. Building on this SGM model developed in 2003, Chopping et al. (2006) sought to use a non-linear SGM model in order to account for upper canopy and background influences. With some assumptions to the SGM, it was determined that angular signals from Compact High Resolution Imaging Spectrometer (CHRIS) imagery could be used to map fractional coverage of wood shrub.

A vegetation index is the reduction of measurements into single values for the purpose of predicting and assessing various characteristics (biomass, percent ground coverage, plant stress, etc.). Because vegetation reflects more strongly in the near-

infrared than in the visible, several forms of vegetation indices have been developed in order to examine the difference in the near-infrared and red channels. Taking the ratio of near-infrared and red bands, Jordan (1969) developed the Ratio-based Vegetation Index (RVI=near-infrared/red). The RVI was first used to measure the leaf-area index of a forest floor. Building on this, Rouse et al. (1973) developed the Normalized Difference Vegetation Index (NDVI; NIR-R/NIR+R) to examine the differences in healthy and unhealthy vegetation. The NDVI is base on the observation that healthy vegetation absorbs most visible light and reflects a large portion of near-infrared light while unhealthy vegetation reflects most visible light and absorbs near-infrared light the NDVI formula was developed. NDVI is calculated by taking the difference in near-infrared and red and dividing it by the sum of near-infrared and red. The resulting values, by definition, are typically between -1 and 1, with 1 being considered very healthy vegetation.

The concept of NDVI and the understanding of basic spectral features of green vegetation have led to the development of various indices that use remote sensing techniques in order to understand and describe vegetation. Richardson and Wiegand (1977) developed the perpendicular vegetation index (PVI), which, like the NDVI examines the differences in the NIR and red channels. The PVI is used to determine vegetation density based on the perpendicular distance from the baseline in each NIR-red plot. This technique is based on the assumption that increasing vegetation density causes an increase in reflectance in the NIR-red channels and these variations are then parallel to

the baseline of the soil. Once the distance of the pixel is determined an estimated vegetation density can be made.

There have been several studies focusing on the loss of wetlands and coastal marshes at the subpixel level (Schmid et al., 2004; Rogers and Kearney, 2003). By applying a normalized difference transformation to Landsat Thematic Mapper (TM) imagery, Rogers and Kearney, studying Atlantic Coast marshes, were able to reduce the spectral variability of soils, water and vegetation while estimating fractional representation. Additionally, they determined that a standard set of endmembers could be applied to all scenes. This technique ensures output consistency and allows for unmixing of scenes devoid of pure pixels. Schmid et al. (2004), used a spectral library and spectral unmixing to examine the degradation of a semi-arid wetlands in central Spain. Using Landsat Enhanced TM (ETM+) and TM data, Schmid et al. developed a multi-temporal analysis to effectively show the rapid degradation to surface cover as a result of human influences and interactions.

Asner and Heidebrecht (2002) used a spectral unmixing model to effectively compare multispectral and hyperspectral observations in the Chihcuahuan Desert of New Mexico. They separated images into classes of photosynthetic vegetation (PV), non-photosynthetic vegetation (NPV) and bare soil. What they found was that measurements in the spectral region of 2.0-2.3 μm, provided the most accurate results when estimating the fractional cover of PV, NPV and bare soil in an arid ecosystem.

Multispectral and multiangular approaches have been effective in monitoring certain types of vegetation and in identifying inundated areas. However, studies that

have incorporated both approaches to monitor and detect changes in wetland vegetation are lacking.

Some Definitions of Reflectance

For clarity in the following sections, definitions of reflectance quantities are provided here. Reflectance is a term that has imprecise meaning, but for accurate understanding one needs to consider the geometries of both the illumination and sensor. This investigation uses the terminology as explained by Hapke (1993). Solar illumination can be direct beam, such as at the top of the atmosphere. It may also be a combination of direct beam and diffuse skylight such as at the surface of the earth. In the former case, the illumination is considered "directional" because it has only a direct component and the direction is a function of the solar zenith and azimuth angles. At the earth's surface, the illumination is considered "hemispherical" because of the addition of the diffuse component.

When reflected energy is viewed from a spaceborne sensor that has a narrow field-of-view, the viewing geometry is also considered directional. Thus, the reflectance measured at the top of the atmosphere is considered Directional-Directional (or "Bidirectional") Reflectance where the first term corresponds to the nature of the illumination and the second corresponds to the nature of the sensor field-of-view. When the Bidirectional Reflectance of a surface is measured relative to that of a diffuse reflector (such as a calibrated panel) it is called the Bidirectional Reflectance Factor (BRF). Specifically, the BRF is the ratio between the spectral radiance at an angle to the object of interest and the spectral radiance of a diffuse reflector at the same angle within

the scene. The Hemispherical-Directional Reflectance is what is measured at the earth's surface: the illumination is hemispherical and the viewing is directional. Specifically, the Hemispherical-Directional Reflectance is a ratio of the radiance reflected by the surface in a specific direction to that reflected (in the same direction) by a perfect Lambertian surface under the same ambient illumination.

Methodology

The overall approach of this study is to incorporate both multispectral and multiangular imagery in order to detect changes in vegetation density and inundated area in the Mesopotamian Marshlands of southeastern Iraq. By using an "angular signature", multiangular data can be used to infer vegetation structure and density. An "angular signature" (Figure 3) is the change in reflectance as a function of the viewing angle. Angular signatures provide information about the amount of vegetation present as well as the underlying surface (water vs. soil). Signatures range from the uniformly distributed (1-dimensional; bowl shape; typically sparse vegetation, no shadows) to complex (3-dimensional; bell shaped; typically abundant vegetation, shadows) (Pinty et al., 2002).

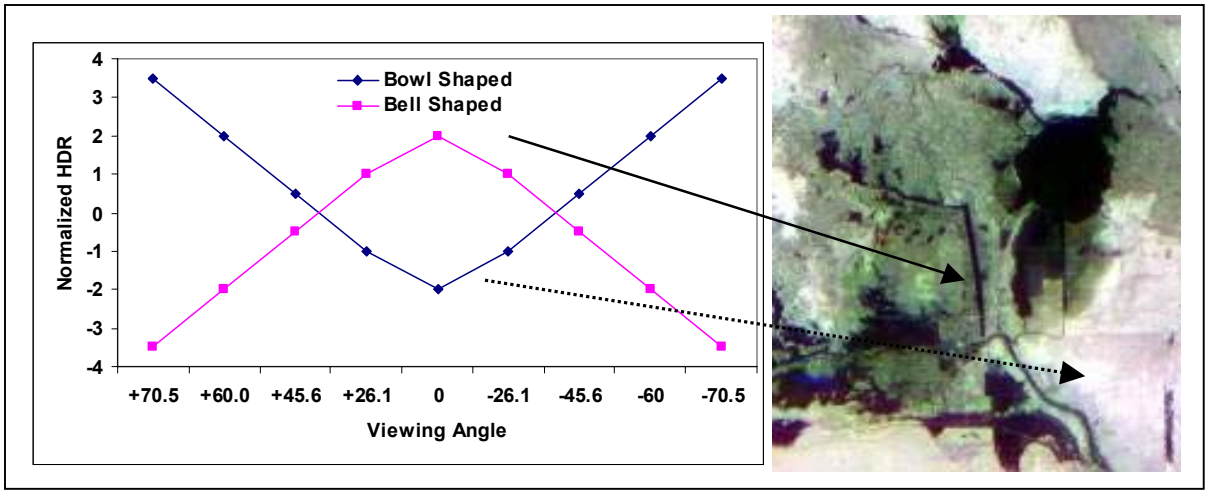

Figure 3. "Bowl" shaped and "bell" shaped angular signatures as described by Pinty et al, 2002.

New Method for Mapping Vegetation Density Using Multiangle Remote Sensing

The Multiangle Imaging SpectroRadiometer (MISR) was launched in December 1999. MISR (Table 3) is an instrument that measures Earth's brightness in four spectral bands (red, blue, green, and near infrared) at each of nine look angles in the forward and aft directions along the flight path. Spatial samples are acquired every 275 meters. Over a period of seven minutes, a 360-km wide swath of Earth comes into view over the nine angles (Diner et al., 1998).

Table 3. Spatial characteristics of the MISR satellite instrument.

Camera Angles	**±70.5^o (Df and Da); ±60.0^o (Cf and Ca); ±45.6^o (Bf and Ba); ±26.1^o (Af and Aa); 0 ^{o} (An);**
Spectral Bands	448 nm (Blue), 558 nm (Green), 672 nm (Red), 866 nm (near IR)
Pixel Size	275 × 275 m (all bands in nadir camera and red bands in all other cameras)
	1.1× 1.1 km (blue, green, and near IR bands in fore and aft cameras)
Swath Width	360 km
Quantization	14 bits, square-root encoded to 12 bits

MISR data used in this study were Level 1B2 terrain-registered at-sensor radiances (L1B2T). Cloud-free MISR images from the spring 2000 to 2005 were used to assess interannual changes in the Mesopotamian Marshlands. Images were converted to top-of-the atmosphere (TOA) hemispherical-directional reflectance factor (HDRF), and then atmospherically corrected using dark pixel subtraction.

Examples of MISR imagery can be seen in Figures 4a and b. These figures show mosaicked MISR images of the Marshlands, while Table 4 provides image characteristics as well as orbit numbers and dates corresponding to images used in this study.

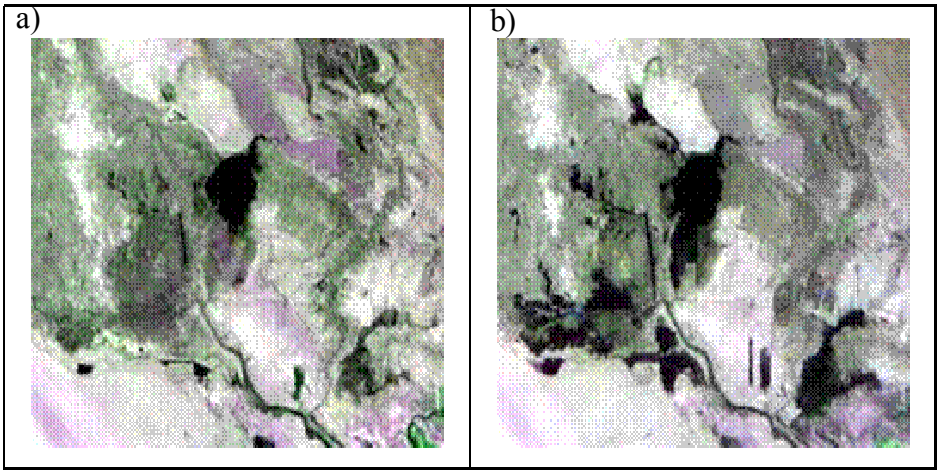

Figure 4. False color composites (bands 12, 7, 2 as R, G, B) of MISR satellite imagery a) 2000 and b) 2005.

Table 4. Dates and orbit numbers of the MISR images used in this study.

Date	Orbit Number
29 May 2000	2373
01 June 2001	7732
03 May 2002	12625
07 June 2003	18450
4 May 2004	23576
11 May 2005	28702

Linear Spectral Unmixing

To estimate vegetation density, the atmospherically corrected MISR imagers are used as input into a linear spectral unmixing model. Linear spectral unmixing is a technique that is commonly used to classify images at the subpixel level (Adams et al., 1986; Asner et al., 1997; Hu et al., 1999; Petrou and Foschi, 1999).

Linear spectral unmixing computes the contribution of image "endmembers" (pure examples of individual scene elements) to the overall pixel reflectance based on the following equation:

$$R_c = \sum_{i=1}^{n} R_{i,c} f_i + \varepsilon_c \qquad \text{Equation 1.}$$

where, R is the reflectance at the i^{th} endmember, $R_{i,c}$ is the reflectance of endmember i at the c channel, f is the fraction of the i^{th} endmember, c is the channel and ε is the error for channel c and n is the number of spectral endmembers (Figure 5a).

a) 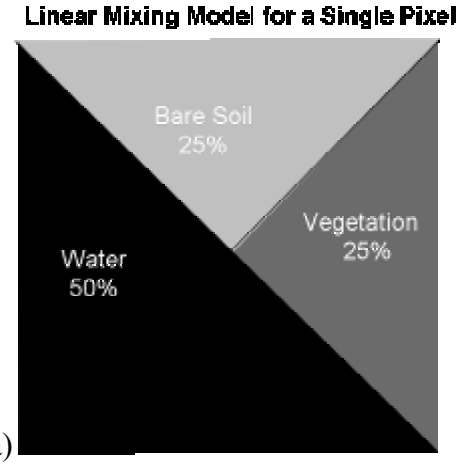

b) 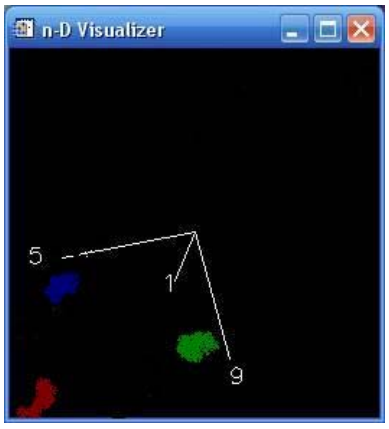

Figure 5. a) Linear spectral unmixing model for a single pixel. (Adapted from Figure 11-15a, Jenson, 2005). b) a 3-axis (3 spectral band) visualization of three endmembers, which are shown by points grouped in multispectral space.

Based on the spectral characteristics that are depicted in images, linear spectral unmixing has the ability to determine relative abundances of materials. The linear spectral unmixing method assumes that reflectance values (at each pixel) are linear combinations of the reflectance of endmembers present within the pixel. The linear spectral unmixing solves for the abundance values of each endmember for every pixel. The number of endmembers selected must not exceed the number of bands available. Therefore linear spectral unmixing results are highly dependent on the selected endmembers (Zhu, 2005).

To assist in endmember selection, each image underwent a Minimum Noise Fraction (MNF) data transformation. The MNF is similar to a principal components transformation, in that the resulting bands are orthogonal and can be used to reduce the dimensionality of a data set, but with the additional benefit of segregating effects due to image noise (Green et al., 1988, Chen et al. 2003). Selected endmembers are then imported into ENVI's "n-dimensional visualizer" (Figure 5b), an interactive scatter-plot model that allows for real-time rotations of the endmembers in n-dimensions (Boardman et al., 1995). This simulation provides the user with the capability to use all bands in an interactive analysis and allows for selection of pure homogeneous pixels (endmembers).

After endmembers are selected the linear spectral unmixing algorithm uses a least squares procedure to solve for the fractions of each endmember in each pixel. Resulting images appear as a series of gray-scale images (one for each endmember). Additionally a root-mean-square error (RMSE) image is also produced, which describes the fit of the linear model to the image data. Brighter pixels in each endmember image represent

higher abundances, whereas brighter pixels in the RMSE image represent higher errors (Boardman et al., 1995, Chang and Ren 2000).

Linear spectral unmixing methods have successfully been applied in wetland regions (Schmid et al., 2004; Rogers and Kearney, 2003) and in arid environments (Asner and Heidebrecht (2002). These results are encouraging and suggest that studies conducted in the Mesopotamian Marshlands can provide similar results and allow for vegetation and water densities to be effectively monitored in this region.

Assessment of Results

High spatial resolution QuickBird imagery provides the foundation for assessment by comparing co-located areas in both the QuickBird and MISR images. QuickBird, launched in 1999, acquires multispectral images in four bands, blue (450 to 520 nm), green (520 to 600 nm), red (630 to 690 nm), and near-IR (760 to 890 nm) at a pixel resolution of approximately 2 meters (Digital Globe, 2005). Because field reconnaissance was not an option for this study, the high spatial resolution provided by QuickBird serves as a proxy for "ground truth".

The two QuickBird images that are used in this study can be seen in Figures 6a and b. Image characteristics for the QuickBird scenes are shown in Table 5.

Table 5. Data characteristics of the QuickBird imagery

Date Acquired	Catalog ID	Center Location	Cloud Cover	Viewing Zenith	Instantaneous Field of View	Area (km^2)
27 April 2002	10100100005C2A01	31.5330N, 47.6849W	0%	8º	2.44m	313
28 May 2005	101001000445301	30.8765N, 47.5096W	0%	8º	2.44m	297

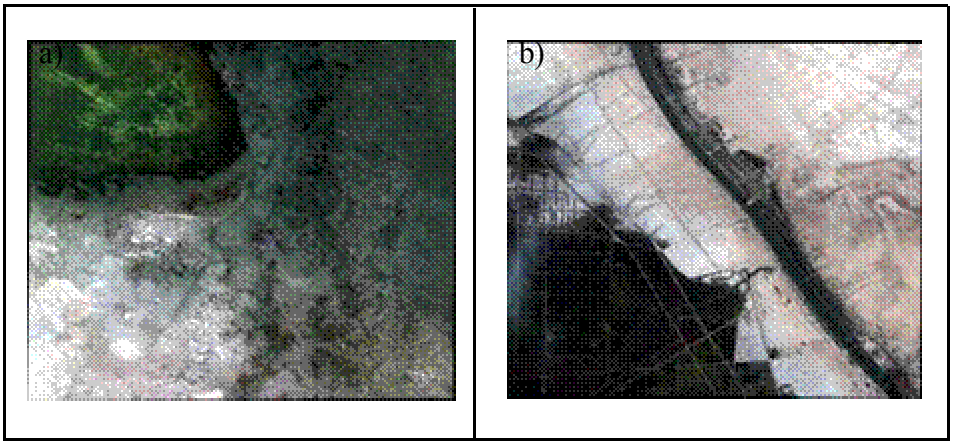

Figure 6. True color-composite QuickBird images a) 2002, b) 2005.

Preprocessing

The two QuickBird images were converted from digital number to top-of-atmosphere (TOA) bidirectional reflectance and then atmospherically corrected using dark pixel subtraction. This procedure creates images of surface hemispherical-directional reflectance (HDR). For each QuickBird image, endmembers were selected and fractional images were computed using spectral linear unmixing using the method described earlier (Equation 1). The endmembers that were used were: vegetation, water, soil, and other.

Validation

The resulting vegetation and water fractional images were compared with those derived from the MISR data. Four sets of comparisons were performed: 1) QuickBird vegetation vs. MISR multispectral vegetation; 2) QuickBird vegetation vs. MISR multiangular vegetation; 3) QuickBird water vs. MISR multispectral water; and 4) QuickBird water vs. MISR multiangular water. All comparisons were performed on a pixel-by-pixel basis with the MISR results resampled to the 2-m QuickBird resolution (using a nearest-neighbor resampling). This step was performed using the ENVI Layer Stacking tool.

Results and Discussion:

Results of the multispectral + multiangular MSR linear spectral unmixing model for vegetation and water are illustrated in Figures 7 and 8. Each figure is composed of six images, one from each of the years 2000 through 2005. Data values associated with each image are found in Table 6. Additionally Table 7, shows the percent change, from one year to the next, for each of the four thresholds (20-40%, 40-60%, 60-80%, and 80-100%) and the root-mean-square-error (RMSE) for each image. Table 6 is also shown in graphic form in Figures 9 and 10.

Figures 11 and 12 show the results of the linear spectral unmixing model for vegetation and water. Data values associated with each image are found in Table 8. Table 9 shows the percent change from one year to the next for each of the four thresholds. Table 8 is also shown in graphic form in Figures 15 and 16. Spectral signatures of vegetation and water are shown in Figures 15 and 16.

The vegetation and water multiangular MISR results are shown in Figures 17 and 18. Data values associated with each image are found in Table 10. Percent changes for each threshold are shown in Table 11 as well as the RMSE for each image. Figures 19 and 20 show in graphic form what is listed in Table 10. Angular signatures of vegetation and water are shown in Figures 15 and 16.

The linear spectral unmixing results for multiangular (Figure 17), multispectral (Figure 11), and multispectral + multiangular (Figure 7) indicate that from 2000 to 2005 there is an increase in the overall amount of vegetation coverage. The multispectral + multiangular image shows that there was an increase of over 421%, as vegetation

increased by over 8821 km^2 from 2096 km^2 in 2000 to 10971 km^2 in 2005 (Tables 6 and 7). Using only the multispectral subset, we see an increase of 135% from 1587 km^2 in 2000 to 3736 km^2 in 2005 (Tables 8-9). Additionally, the multiangular subset indicates that there was an increase of 44%, from 9787 km^2 in 2000 to 14,098 km^2 in 2005 (Tables10 and11).

Water coverage for the area has also shown a significant increase in two of the images, and a significant decrease in one of the images. In 2000 the multispectral + multiangular image showed that water accounted for 616 km^2 and by 2005 it had increased 572% to account for an area of 4139 km^2 (Tables 6-7). The multiangular subset indicated that there was an increase of 1079% from 1570 km^2 in 2000 to 18515 km^2 by 2005 (Tables 10 and 11). Meanwhile, the multispectral subset showed a decrease of 86% from 9255 km^2 to 1304 km^2 (Tables 8-9).

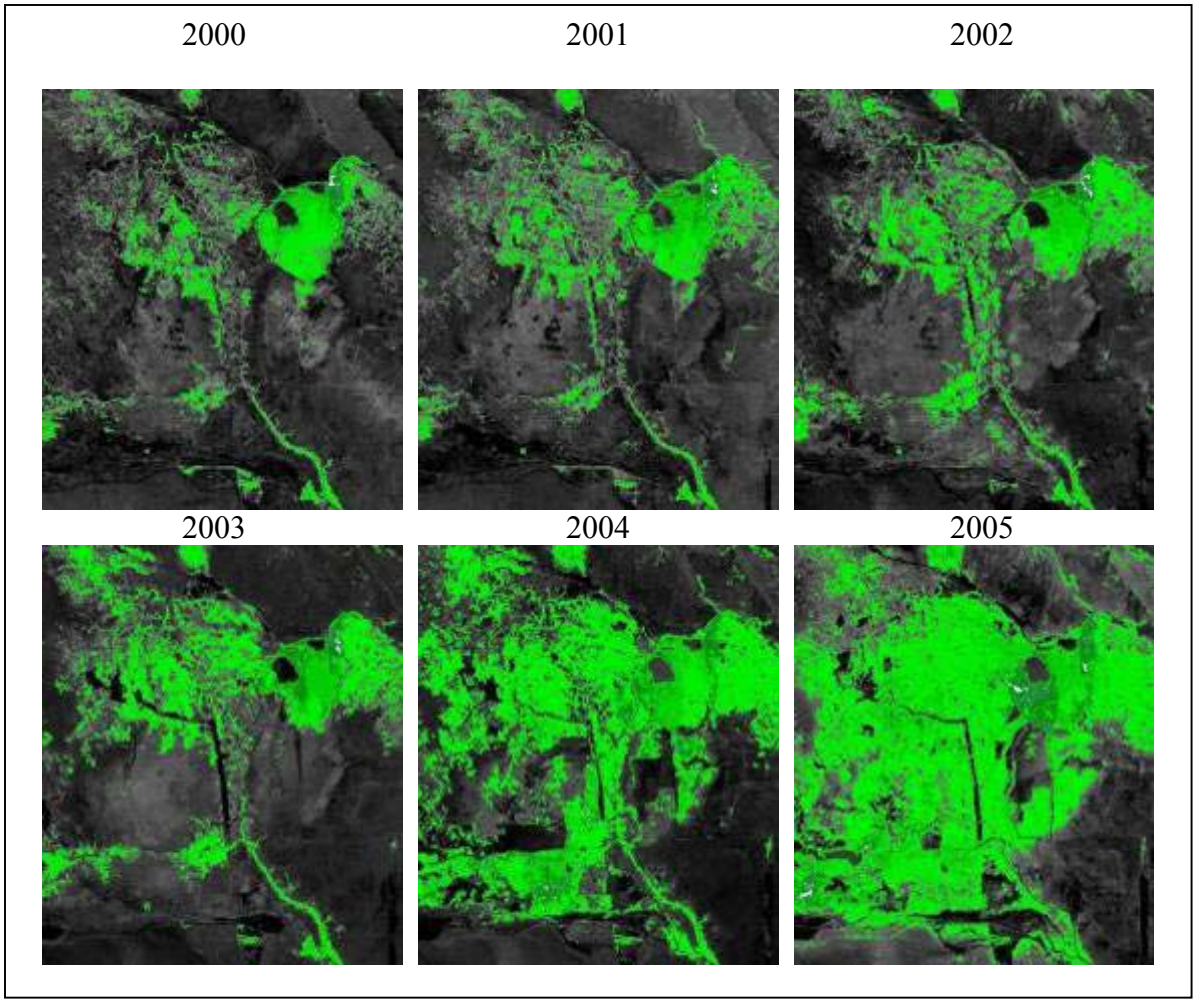

Figure 7. Linear spectral unmixing image results for vegetation coverage: multispectral + multiangular. Green areas show pixels having a vegetation fraction of at least 20%.

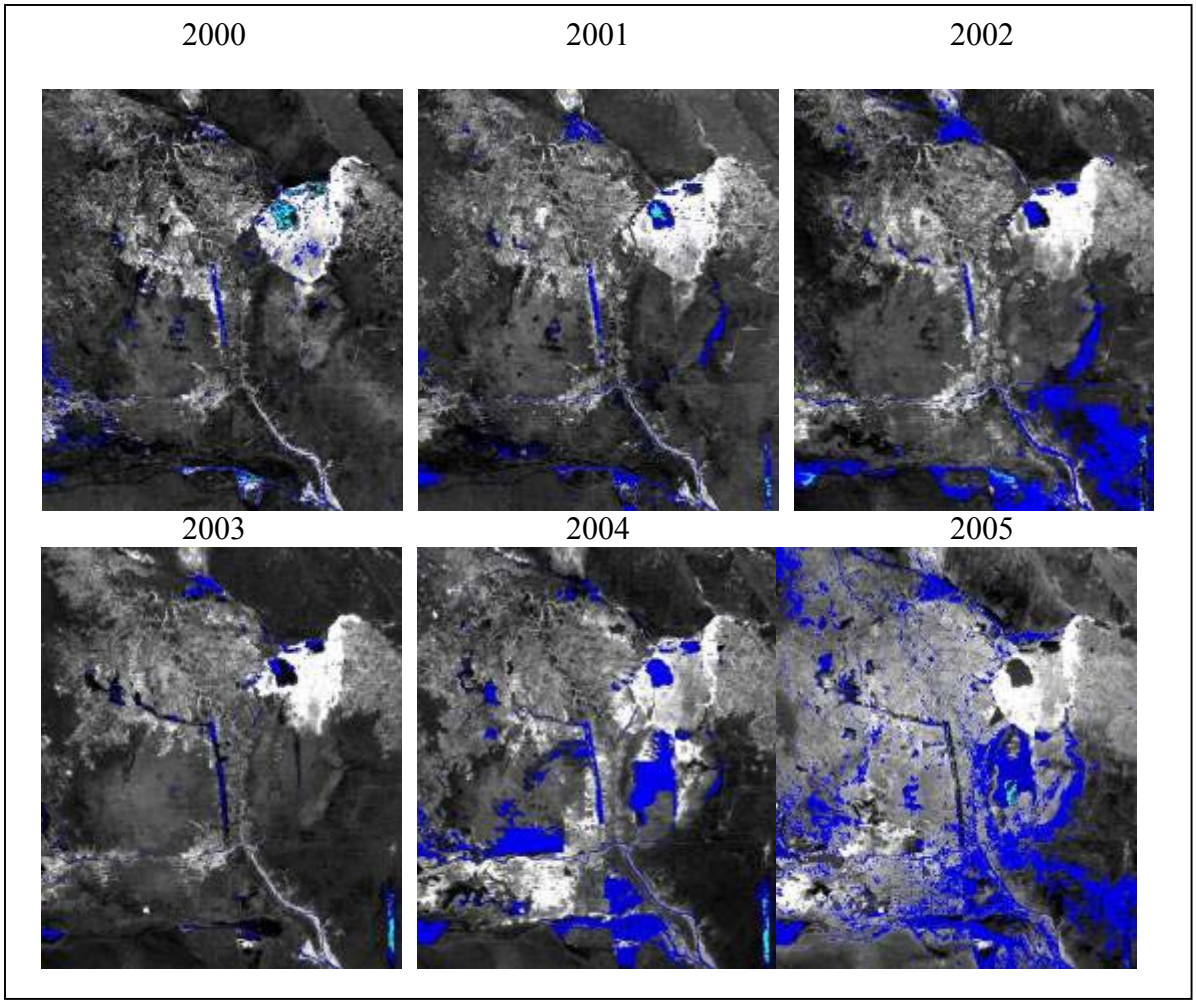

Figure 8. Linear spectral unmixing image results for water coverage: multispectral + multiangular. Blue areas show pixels having a water fraction of at least 20%. Cyan areas show pixels having a water fraction of at least 80%.

Table 6. Percent coverage as a result of spectral linear unmixing: multispectral + multiangular

Vegetation Area by Percent Cover (km^2)						
	20%-40%	40%-60%	60%-80%	80%-100%	Total	RMSE
Date						
29 May 2000	1446	335	76	39	2096	.0061
01 June 2001	1987	442	128	45	2602	.0039
03 May 2002	2677	386	94	46	3203	.0040
07 June 2003	3223	439	191	43	3896	.0057
24 May 2004	6137	1289	435	106	7967	.0053
11 May 2005	8102	2185	445	183	10917	.0059
Water Area by Percent Cover (km^2)						
	20%-40%	40%-60%	60%-80%	80%-100%	Total	RMSE
Date						
29 May 2000	346	128	71	71	616	.0061
01 June 2001	433	130	53	29	645	.0039
03 May 2002	1563	214	97	43	1917	.0040
07 June 2003	267	38	16	21	341	.0057
24 May 2004	1547	326	26	27	1925	.0053
11 May 2005	3473	543	103	20	4139	.0059

Table 7. Yearly percent change based on results of spectral linear unmixing: multispectral + multiangular.

Vegetation Area by Percent Area (km^2)					
	20%-40%	40%-60%	60%-80%	80%-100%	Total
Date					
2000-2001	37	32	69	15	24
2001-2002	35	-13	-27	2	23
2002-2003	20	14	103	-7	22
2003-2004	90	194	128	147	104
2004-2005	32	70	2	77	37
Water Area by Percent Area (km^2)					
	20%-40%	40%-60%	60%-80%	80%-100%	Total
Date					
2000-2001	25	2	-25	-59	5
2001-2002	261	65	83	48	197
2002-2003	-83	-82	-84	-51	-82
2003-2004	479	758	63	27	465
2004-2005	125	67	296	-26	115

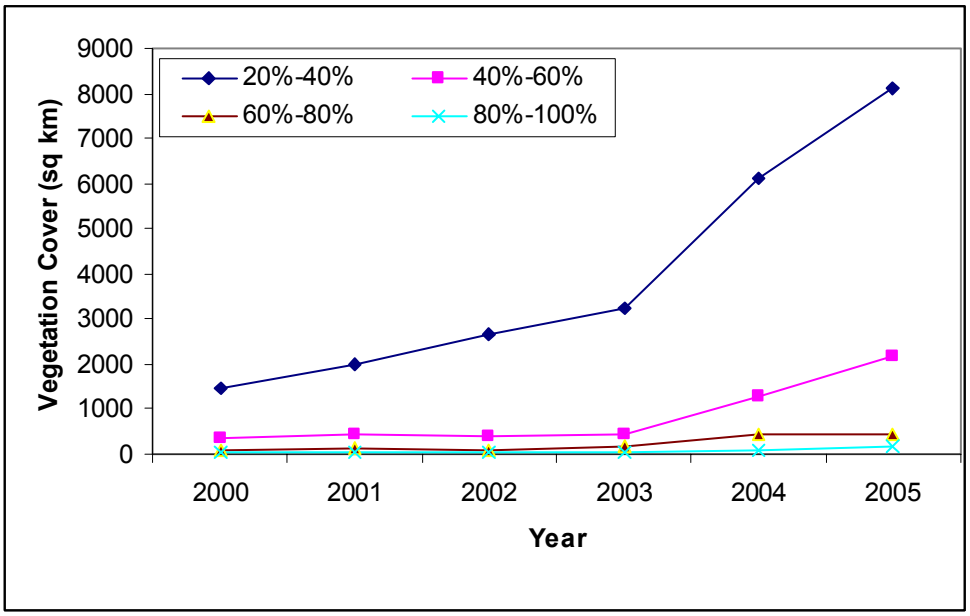

Figure 9. Extent of vegetation (by percent cover) from 2000-2005 for pixels with fractional cover of at least 20%: multispectral + multiangular.

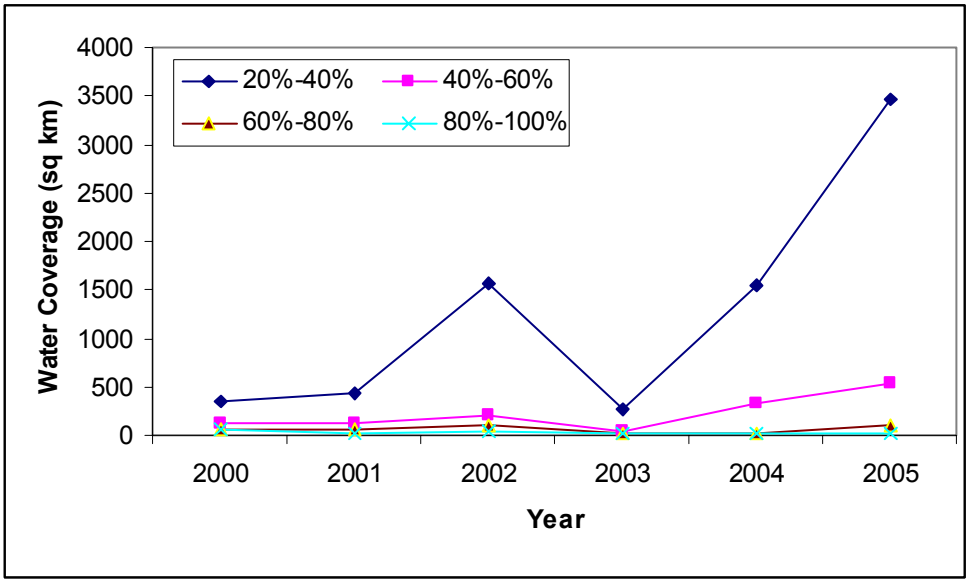

Figure 10. Extent of water (by percent cover) from 2000-2005 for pixels with fractional cover of at least 20%: multispectral + multiangular.

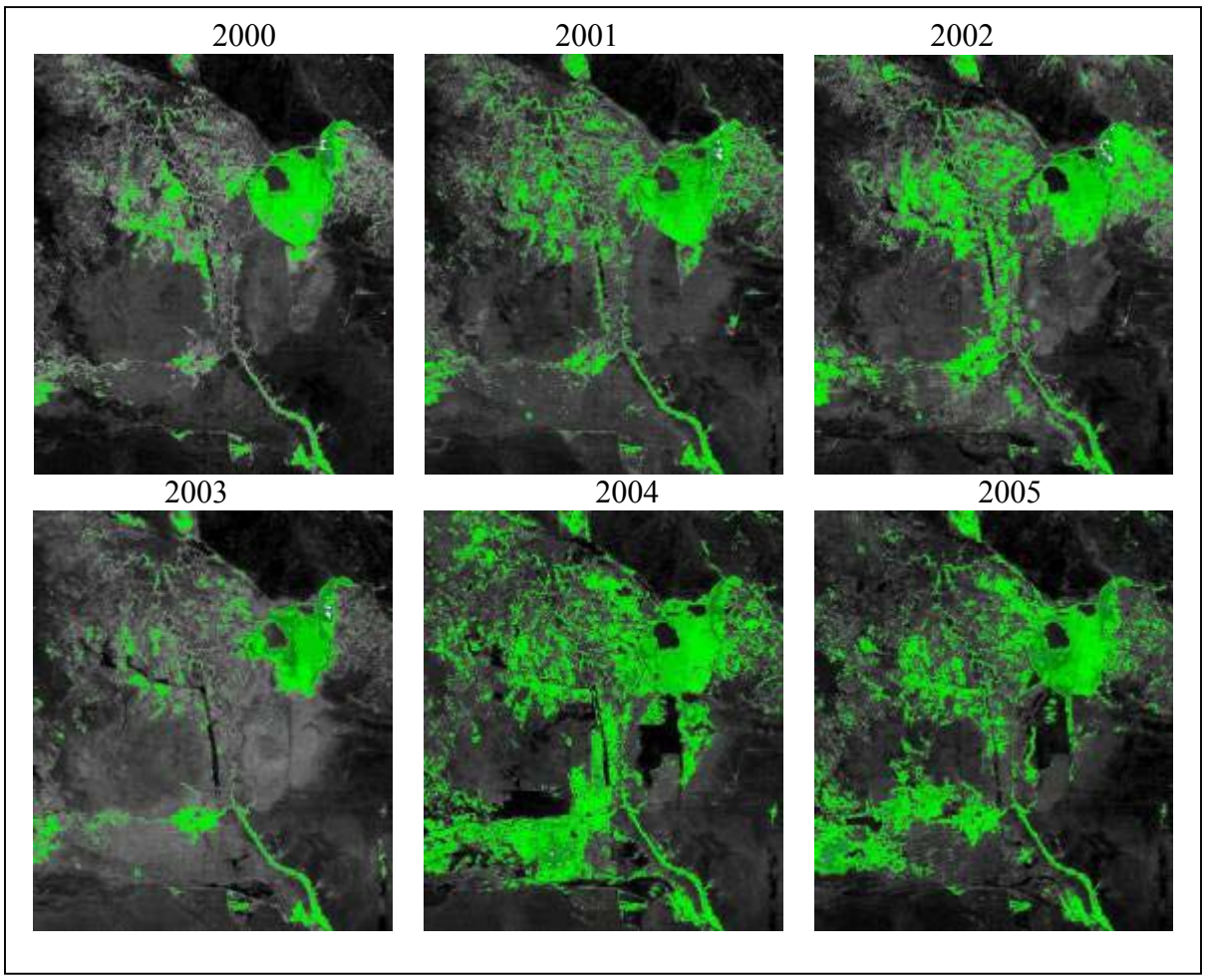

Figure 11. Linear spectral unmixing image results for vegetation coverage: multispectral only. Green areas show pixels having a vegetation fraction of at least 20%.

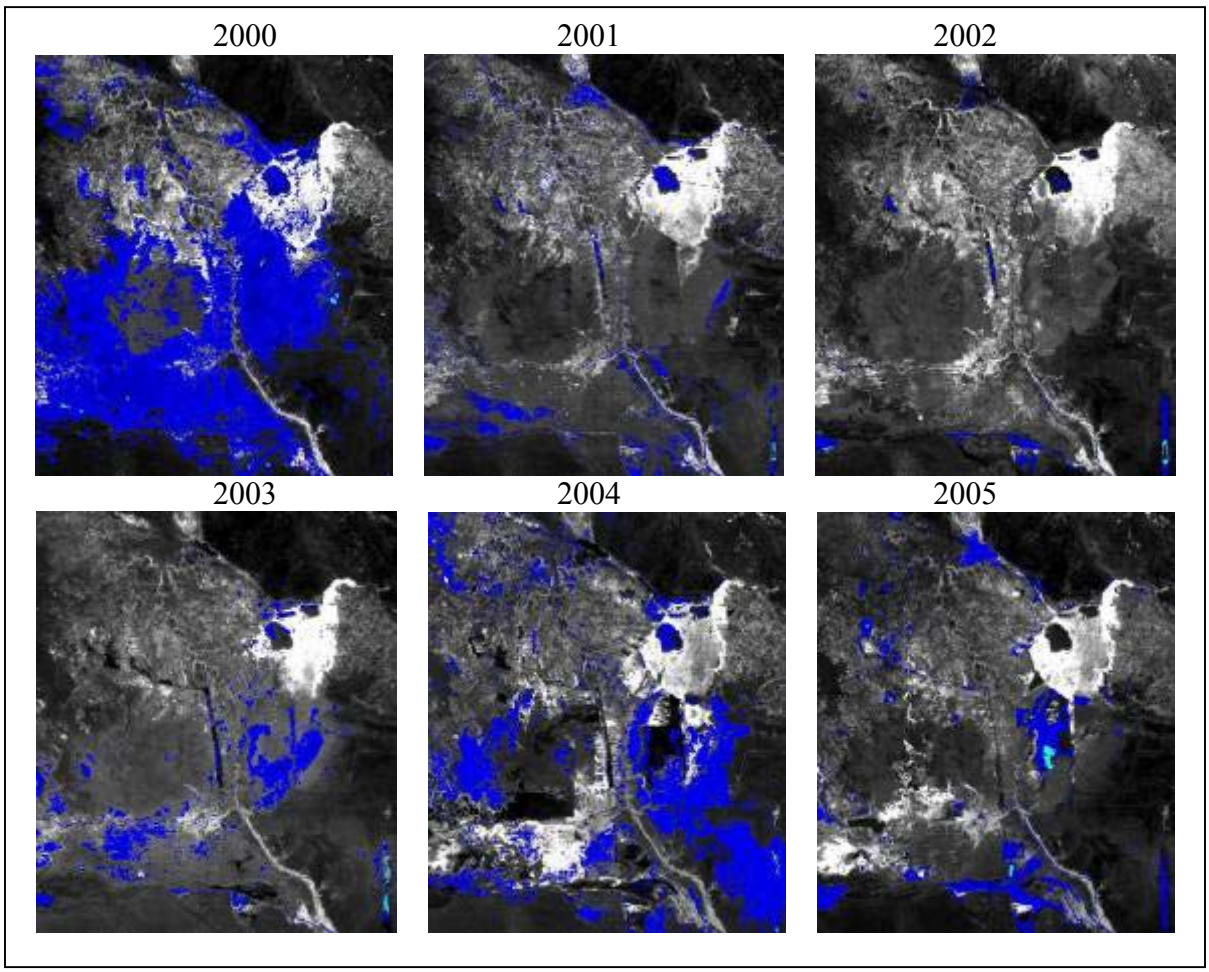

Figure 12. Linear spectral unmixing image results for water coverage: multispectral only. Blue areas show pixels having a water fraction of at least 20%. Cyan areas show pixels having a water fraction of at least 80%.

Table 8. Percent coverage as a result of spectral linear unmixing: multispectral.

Vegetation Area by Percent Cover (km^2)					
	20%-40%	40%-60%	60%-80%	80%-100%	Total
Date					
29 May 2000	1199	285	66	37	1587
01 June 2001	1987	442	127	45	2601
03 May 2002	2502	375	93	46	3016
07 June 2003	938	256	192	46	1432
24 May 2004	3509	999	366	88	4062
11 May 2005	2604	689	329	114	3736
Water Area by Percent Cover (km^2)					
	20%-40%	40%-60%	60%-80%	80%-100%	Total
Date					
29 May 2000	4485	2435	307	31	9255
01 June 2001	433	130	53	29	645
03 May 2002	200	58	24	12	294
07 June 2003	1047	178	22	18	1265
24 May 2004	3582	84	10	7	3683
11 May 2005	944	249	78	33	1304

Table 9. Yearly percent change based on results of spectral linear unmixing: multispectral.

Vegetation Area by Percent Cover (km^2)					
	20%-40%	40%-60%	60%-80%	80%-100%	Total
Date					
2000-2001	66	55	92	22	64
2001-2002	26	-15	-27	2	16
2002-2003	-63	-32	107	0	-53
2003-2004	-274	290	91	91	183
2004-2005	-26	31	-10	30	-8
Water Area by Percent Cover (km^2)					
	20%-40%	40%-60%	60%-80%	80%-100%	Total
Date					
2000-2001	-90	-95	-83	-7	-93
2001-2002	-54	-58	-55	-59	-54
2002-2003	424	207	-8	50	330
2003-2004	242	-53	55	61	191
2004-2005	-73.6	196	680	371	-65

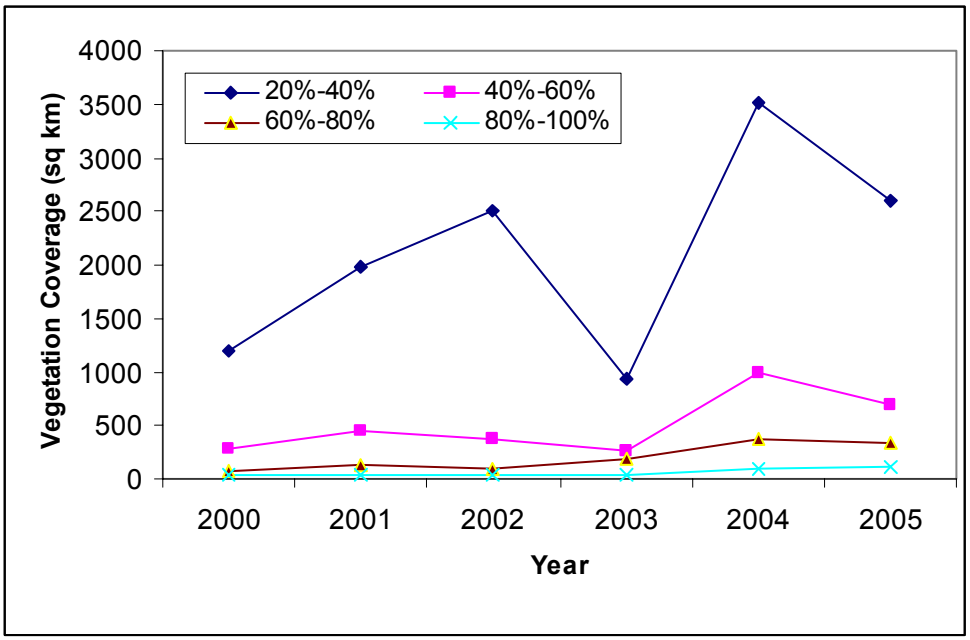

Figure 13. Extent of vegetation (by percent cover) from 2000-2005 for pixels with fractional cover of at least 20%: multispectral

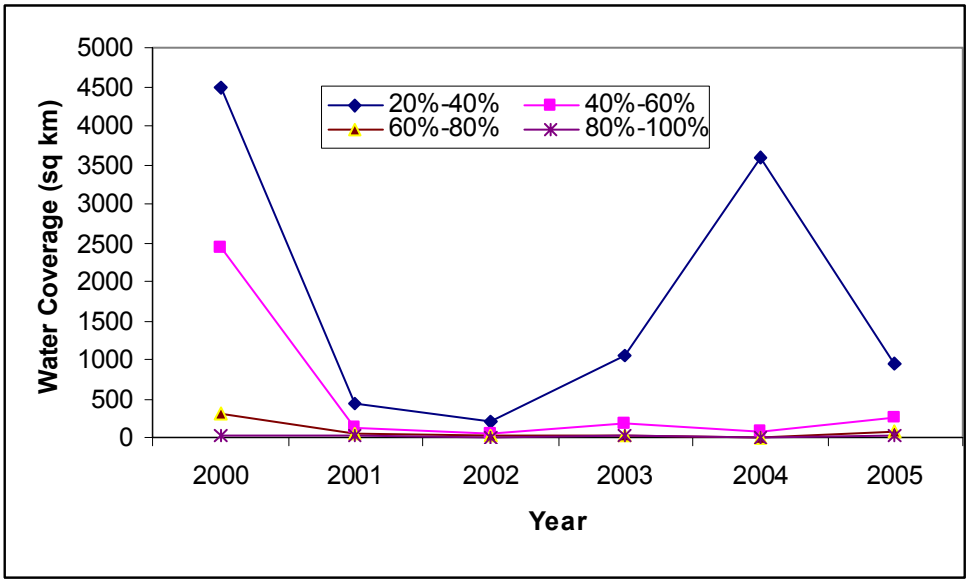

Figure 14. Extent of water (by percent cover) from 2000-2005 for pixels with fractional cover of at least 20%: multispectral

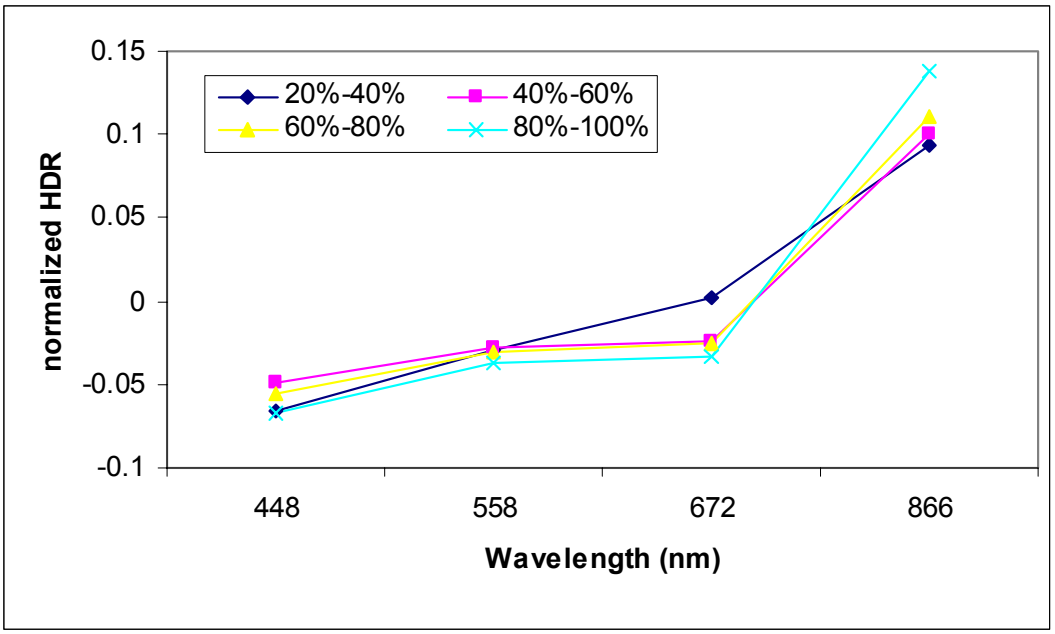

Figure 15. Average spectral signature (2000-2005) for vegetation pixels in MISR multispectral images that have at least 20% coverage.

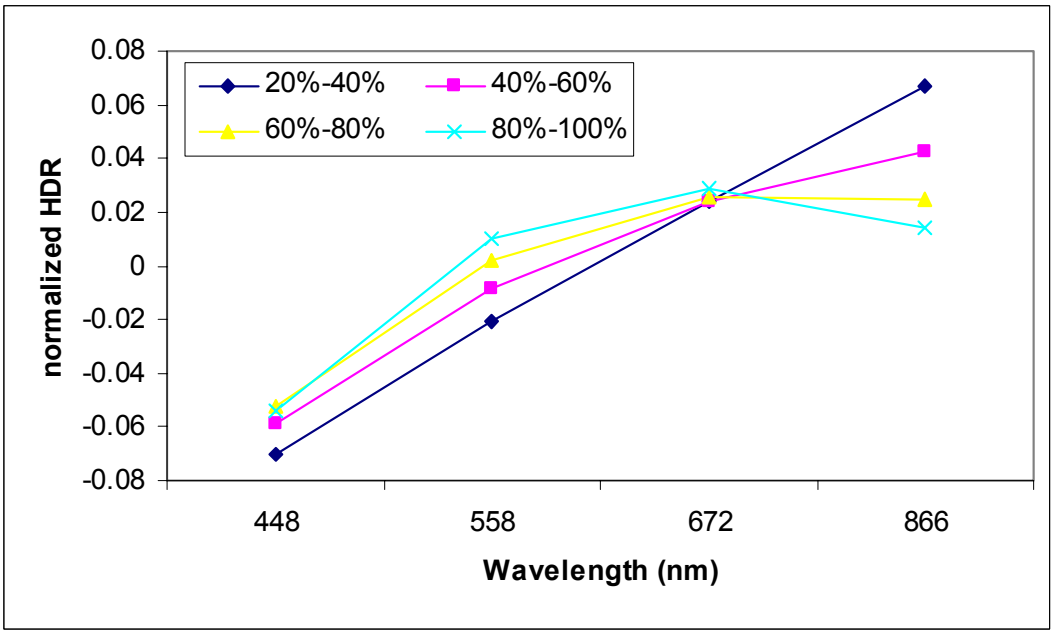

Figure 16. Average spectral signature (2000-2005) for water pixels in MISR multispectral images that have at least 20% coverage.

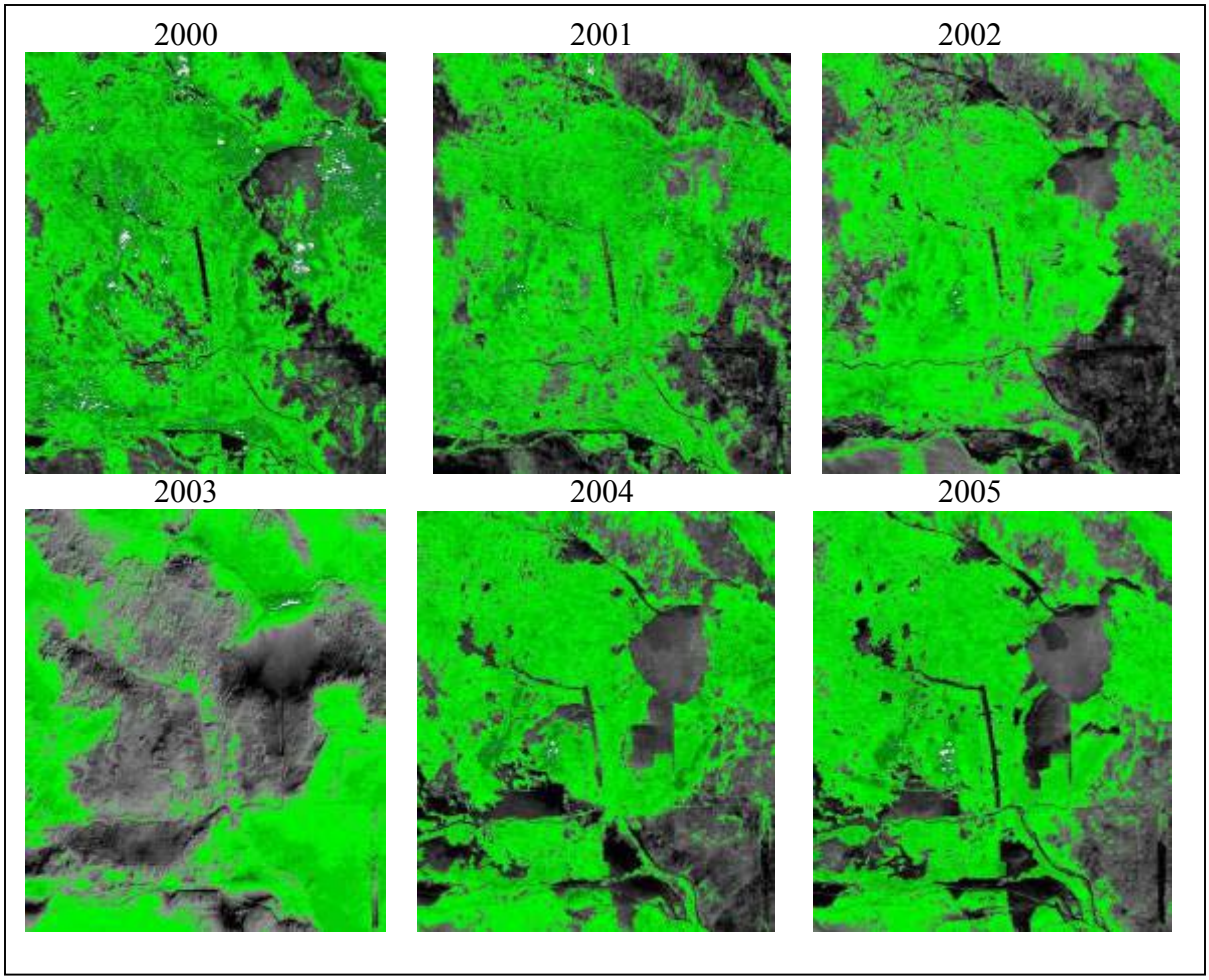

Figure 17. Linear spectral unmixing image results for vegetation coverage: multiangular. Green areas show pixels having a vegetation fraction of at least 20%

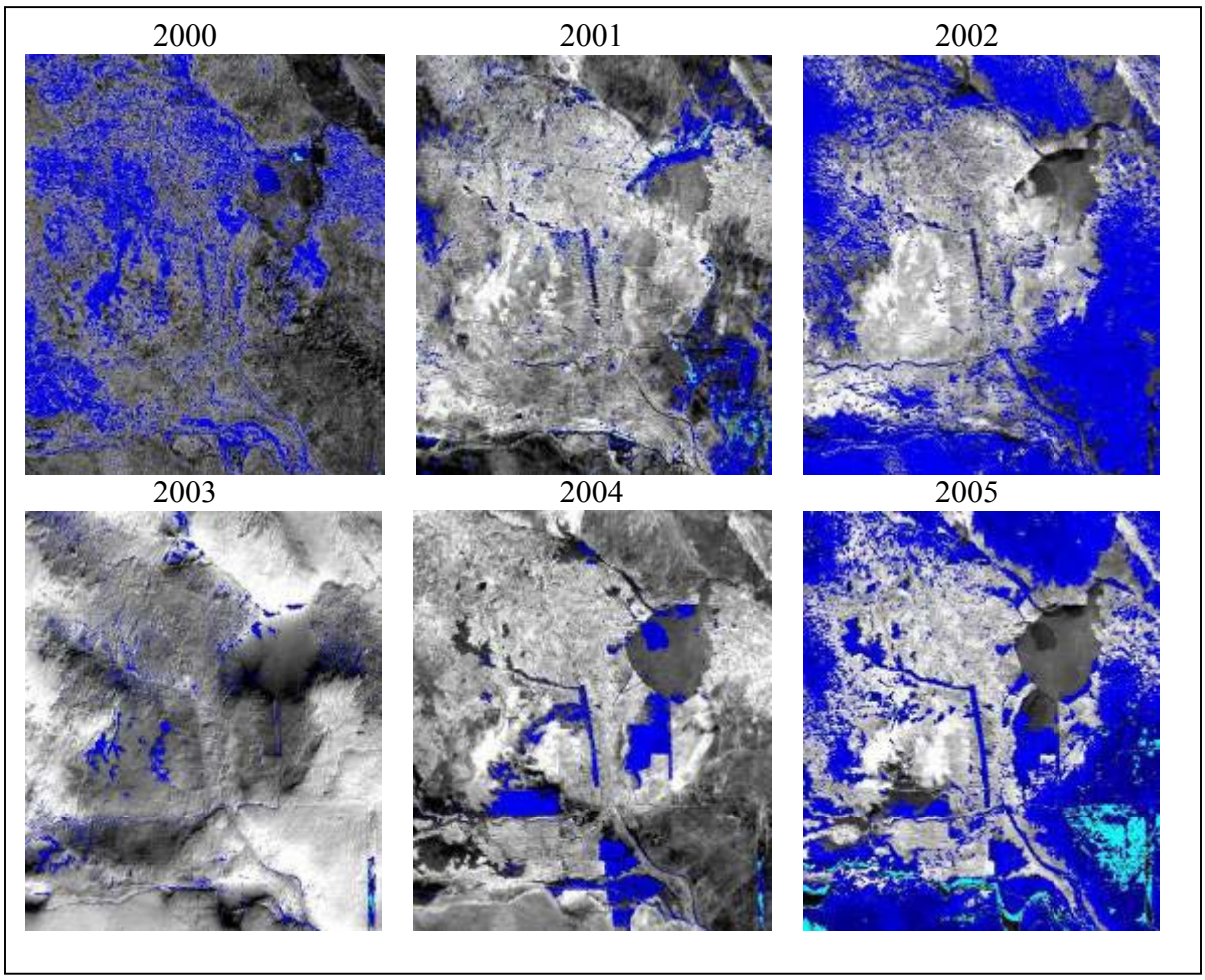

Figure 18. Linear spectral unmixing image results for water coverage: multiangular. Blue areas show pixels having a water fraction of at least 20%. Cyan areas show pixels having a water fraction of at least 80%.

Table 10. Percent coverage as a result of spectral linear unmixing: multiangular.

Vegetation Area by Percent Cover (km^2)						
	20%-40%	40%-60%	60%-80%	80%-100%	Total	RMSE
Date						
29 May 2000	8334	1390	54	9	9787	0.0025
01 June 2001	6811	5115	1563	288	9177	0.0040
03 May 2002	4326	256	16	1	4599	0.0029
07 June 2003	7143	2898	220	40	10301	0.0026
24 May 2004	7510	5134	724	86	13454	0.0031
11 May 2005	8186	5355	496	61	14098	0.0038
Water Area by Percent Cover (km^2)						
	20%-40%	40%-60%	60%-80%	80%-100%	Total	RMSE
Date						
29 May 2000	1222	227	95	26	1570	0.0025
01 June 2001	1054	576	306	154	2090	0.0040
03 May 2002	5989	238	39	42	6308	0.0029
07 June 2003	781	39	22	12	854	0.0026
24 May 2004	995	415	34	16	1460	0.0031
11 May 2005	11442	3463	2773	837	18515	0.0038

Table 11. Yearly percent change based on results of spectral linear unmixing: multiangular.

Vegetation Area by Percent Area (km^2)					
	20%-40%	40%-60%	60%-80%	80%-100%	Total
Date					
2000-2001	-18	268	2794	3100	-6
2001-2002	-36.5	-95	-99	-100	50
2002-2003	65	1032	1275	3900	124
2003-2004	5	77	229	115	31
2004-2005	9	4	-32	-29	5
Water Area by Percent Area (km^2)					
	20%-40%	40%-60%	60%-80%	80%-100%	Total
Date					
2000-2001	-14	154	222	492	33
2001-2002	468	-59	-87	-73	202
2002-2003	-87	-84	-44	-71	-86
2003-2004	27	961	55	6.7	71
2004-2005	1050	735	8056	5131	1168

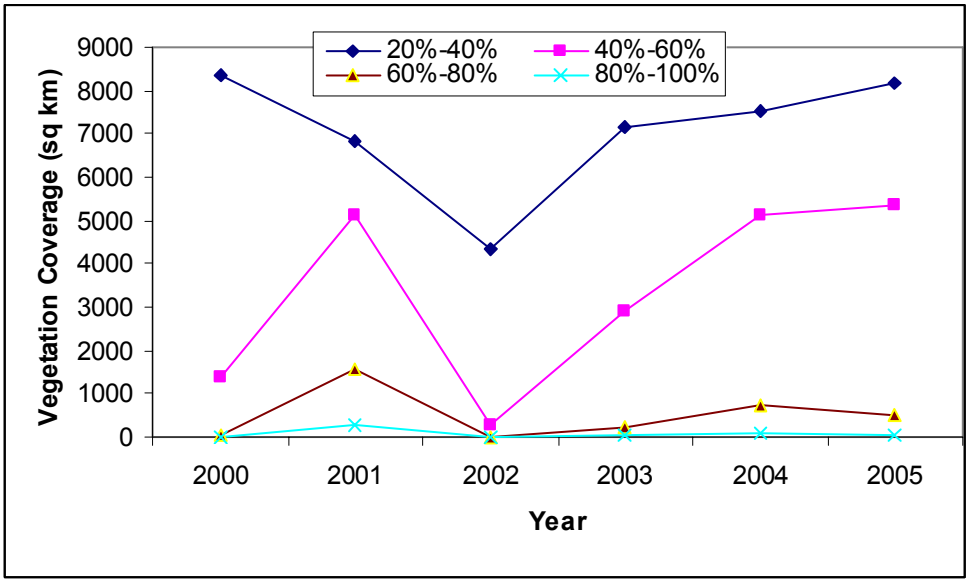

Figure 19. Extent of vegetation (by percent cover) from 2000-2005 for pixels with fractional cover of at least 20%: multiangular

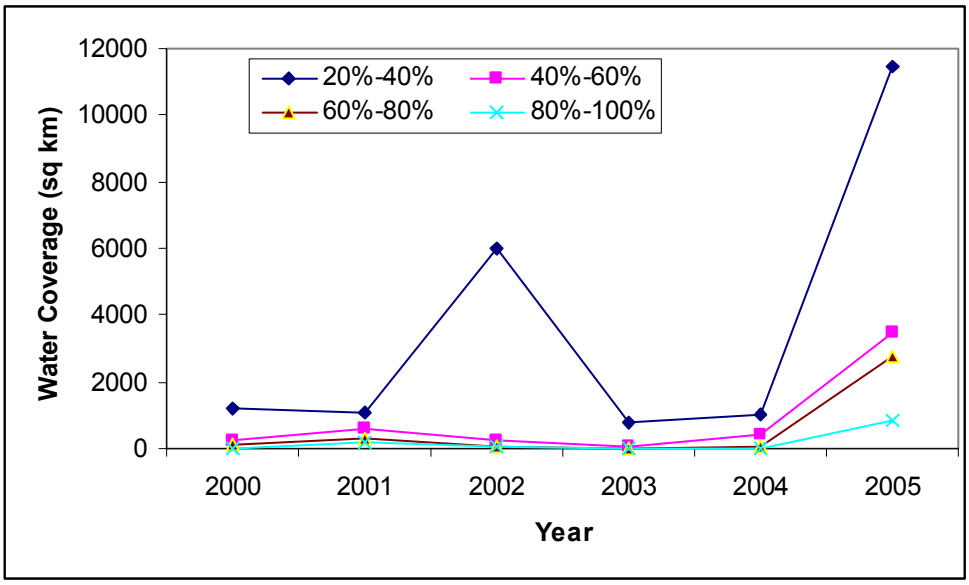

Figure 20. Extent of water (by percent cover) from 2000-2005 for pixels with fractional cover of at least 20%: multispectral.

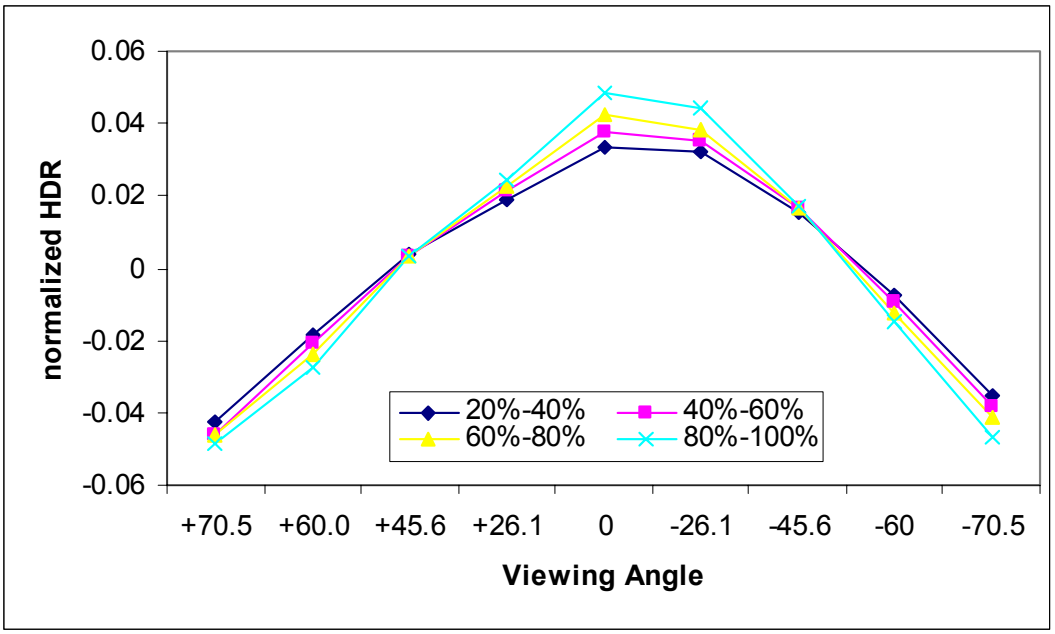

Figure 21. Average angular signature (2000-2005) for vegetation pixels in MISR multiangular images that have at least 20% coverage.

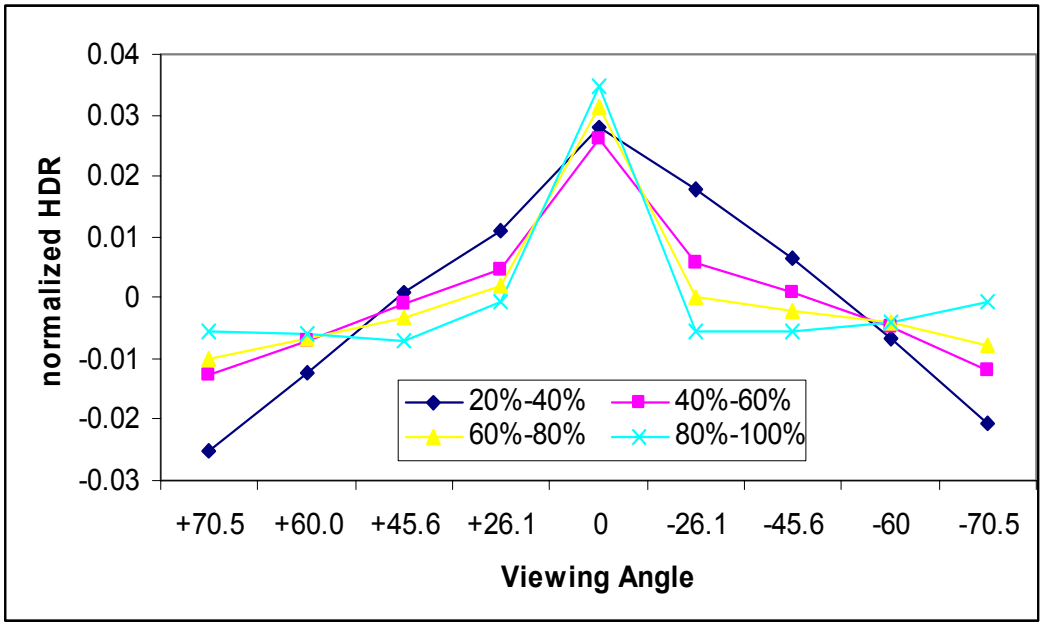

Figure 22. Average angular signature (2000-2005) for water pixels in MISR multiangular images that have at least 20% coverage.

Angular and Spectral Signatures

In order to assess and understand the results obtained from the linear spectral unmixing model, spectral and angular signatures for pixels with a fractional coverage of at least 20% will be examined. An angular signature (Figures 21 and 22) is the change in reflectance as a function of the viewing angle and is typically used to infer vegetation structure and density. For low, sparse vegetation and for uniform, very dense vegetation the angular shape is termed the "bowl shape" (Pinty et al, 2002). For medium density vegetation with a three-dimensional character, the angular shape is termed the "bell shape". As seen in Figure 21 multiangular pixels that were determined to have vegetation densities of 20%-40%, 40%-60%, 60%-80% and 80%-100% have very distinct "bell" shaped angular signatures. For pixels that were determined to be water and had densities of 20%-40% and 40%-60%, the angular signatures are transitional into "bell shaped" signatures. Meanwhile for water densities of 60%-80% and 80% to 100% the angular signatures transition from bowl-shaped in the angular viewing angles to bell-shaped in the nadir-viewing angle.

A spectral signature (Figures 15 and 16) is the specific combination of reflected and absorbed electromagnetic (EM) radiation at varying wavelengths which can uniquely identify an object. A chemical compound in vegetation (chlorophyll) strongly absorbs radiation in the red and blue wavelengths but reflects green and near-infrared wavelengths. Water, meanwhile, may reflect somewhat similarly to vegetation in the visible wavelengths but is almost always separable in the infrared. When examining the spectral signatures for vegetation densities of 40%-60%, 60%-80% and 80%-100%

(Figure 15), we can see high absorptions in the red (672 nm) and the blue (448 nm) and high reflections in the green (558 nm). For vegetation densities of 20%-40%, the spectral pattern tends to follow that of soil (high reflectance in all bands). Due to the low amount of vegetation present, the spectral properties of soil are evident.

Water densities of 60%-80% and 80%-100% follow the patterns of open water described in 2000 when Munyati examined multispectral Landsat imagery to detect changes in wetlands in the Kafue Flats of Zambia. Water densities of 20%-40% and 40%-60% again follow similar patterns of soil suggesting that with the low presence of water, spectral properties of soil are dominant. All of the water signatures have very low normalized HRD values, which suggest that there isn't much reflectance, but rather high absorption that influences the spectral pattern. The reflectance of clear water is generally low. The topography of the water (i.e. rough, smooth floating sediment) increases the reflectance in the red portion of the spectrum.

Validation

Figures 23 through 28 show the comparison of multiangle + multispectral MISR (Figures 23 and 24), multispectral MISR (Figures 25 and 25), and multiangular MISR (Figures 27 and 28) with QuickBird estimates of water and vegetation for 2002 and 2005. White pixels represent areas where specified conditions were met. The conditions considered were: 1) where do both images detect vegetation; 2) where do both images detect water; 3) where does only MISR detect vegetation; 4) where does only MISR detect water; 5) where does only QuickBird detect vegetation; and 6) where does only QuickBird detect water. In all cases, a pixel is considered to contain vegetation or water if either contains a minimum fractional cover of 20%.

Fractional Differences

In order to assess the individual contributions multiangular and multispectral information in mapping the fractions of vegetation and water, the results of each were compared with fractional images from the two QuickBird images.

Pixel-by-pixel comparisons of the 2002 and 2005 images (Figures 23-28 and Table 12) clearly demonstrate the effectiveness of QuickBird to detect vegetation and water. However, the effectiveness of the multiangular and multispectral approaches is the primary interest of this study. In the 2002 image, when compared to the multispectral + multiangular image, QuickBird identified 7 km^2 of vegetation and 218 km^2 of water. When compared with the multispectral subset QuickBird was able to detect 7 km^2 of vegetation and 242 km^2 of water. And when compared to the multiangular subset QuickBird detected 140 km^2 of vegetation and 269 km^2 of water. On the other hand, the

MISR images tended to overestimate vegetation and water. The multispectral + multiangular image overestimated vegetation by 21 km^2 and water by 9 km^2. The multiangular subset overestimated vegetation by 25 km^2 and water by 4 km^2. And the multispectral subset overestimated vegetation by 32 km^2 and water by 0 km^2. However, multispectral + multiangular imagery were able to identify 168 km^2 of vegetation and 18 km^2 of water were the QuickBird image also identified both. The subset images were also able to identify areas that corresponded to QuickBird as multispectral imagery detected 188 km^2 of vegetation and 8 km^2 of water, and multiangular imagery 59 km^2 of vegetation.

The 2005 pixel-by-pixel comparison provided similar results to those of 2002. In 2005, when compared to the multispectral + multiangular image, QuickBird was able to detect 42 km^2 of vegetation and 99 km^2 of water. When compared to the multispectral subset, QuickBird, detected 27 km^2 of vegetation and 128 km^2 of water. Lastly, when compared to the multiangular subset QuickBird detected 49 km^2 of vegetation and 148 km^2 of water. As in the 2002 image, all MISR images tended to overestimate vegetation and water. The multispectral + multiangular image overestimated vegetation by 76 km^2 and water by 15 km^2. The multispectral subset overestimated vegetation by 10 km^2 and water by only 3 km^2. Finally, the multiangular subset overestimated vegetation by 132 km^2 and water by 14 km^2. As in 2002, the 2005 multispectral + multiangular images, multispectral and the multiangular images were all able to identify corresponding pixels in the QuickBird images as vegetation and water. The multispectral + multiangular image detected 14 km^2 of vegetation and 88 km^2 of water, the multispectral image 24

km^2 of vegetation and 28 km^2 of water and the multiangular image 6 km^2 of vegetation and 39 km^2 of water.

When examining the original QuickBird images for 2002 and 2005 (Figure 6a and b), the vast differences in the images are clearly apparent. The 2002 image was acquired directly in the middle of the Hawr al Hawizeh marsh. The majority of this image is composed of various degrees of vegetation, water, soil and various forms of salt flats. Meanwhile, the 2005 image was acquired on the edge of the Hawr al Hammar marsh and includes the city of Bashra. The 2005 image is composed of low amounts of vegetation, water, soil and many areas of human impact. The 2-m spatial resolution of QuickBird proved to be very effective in differentiating between small changes such as roads, housing units, and water diversions, which the coarser resolution MISR images did not show.

Images illustrating fractional differences (MISR multiangular and multispectral images are subtracted from the corresponding QuickBird images) can be seen in Figures 29-36. In addition, each figure contains a histogram showing the data. Histograms are summary graphs that show counts of data points that fall in various ranges. These graphs provide an approximation of the frequency distribution of the data. When looking at the histograms it is important to note that areas shown in white had a high value in the QuickBird images and a low value in the MISR images (for the same pixel represented in each image). Areas shown in a dark color were determined to have a low value in the QuickBird image but a high value in the MISR image. Gray areas show little difference between MISR and QuickBird images.

When examining the histogram for 2005 multispectral vegetation (Figure 30), we can see a Gaussian distribution. This suggests that there are very few differences between the fractional estimates of QuickBird and MISR multispectral vegetation in the 2005 data set. The peak of the histogram occurs at a value of 0.1, indicating that the overall differences between the two images are small.

For the 2005 multiangular vegetation difference image (Figure 29), the histogram shows a bimodal distribution. This indicates that there are two distinct values around which the data tend to be grouped. The two peak values are -0.23 and 0.20. The positive peak of 0.20 in this case is a result of QuickBird classifying a larger amount of area as vegetation (Table 12) than the corresponding multiangular imagery. The negative peak is due to the large amount of vegetation that was classified in the multiangular image, which did not correspond to values of vegetation in the QuickBird image.

Looking at the histogram for fractional differences in water, we again see a bimodal distribution. The two peaks for 2005 multiangular difference image are 0.1 and 0.6. In Table 12, we see that the 2005 QuickBird image maps a greater percentage of the area as water. The histogram peaks at a value of 0.1. Multiangular imagery identified 132 km^2 of water where the QuickBird image was unable to identify any, and this is shown in the second peak (0.6).

The histogram associated with water fractional differences for the 2005 multispectral image appears positively skewed. A positively skewed distribution is representative of data clustering around the lower values with slightly increasingly frequencies towards the larger values. In this particular case we see that there is a peak of

0.1 and then the data tails off to the right. The shape of the distribution can be attributed to QuickBird's ability to detect water (peaks) where the MISR multispectral approach cannot (the tail).

The 2002 vegetation fractional histogram for the multispectral difference (Figure 34) is again a Gaussian distribution with the peak at 0.0. Vegetation fractional differences associated with the 2002 multiangular imagery (Figure 33) are a kurtotic distribution (also known as "super-Gaussian"). The peak associated with this distribution occurs at a value of 0.1 and sharply declines.

Histograms associated with 2002 water fractional differences associated with both multispectral and multiangular imagery are illustrated in Figures 35 and 36 and follow a trimodal distribution. This indicates that they are three distinct values around which the data are grouped. For the multiangular imagery (Figure 35) the three peaks occur at 0.4, 0.6, and 1.0. The peaks associated with the multispectral histogram occur at 0.4, 0.7, and 0.8. These positive peaks are due to the large amount of water that was classified in the QuickBird image, which do not correspond to values of vegetation in the MISR images.

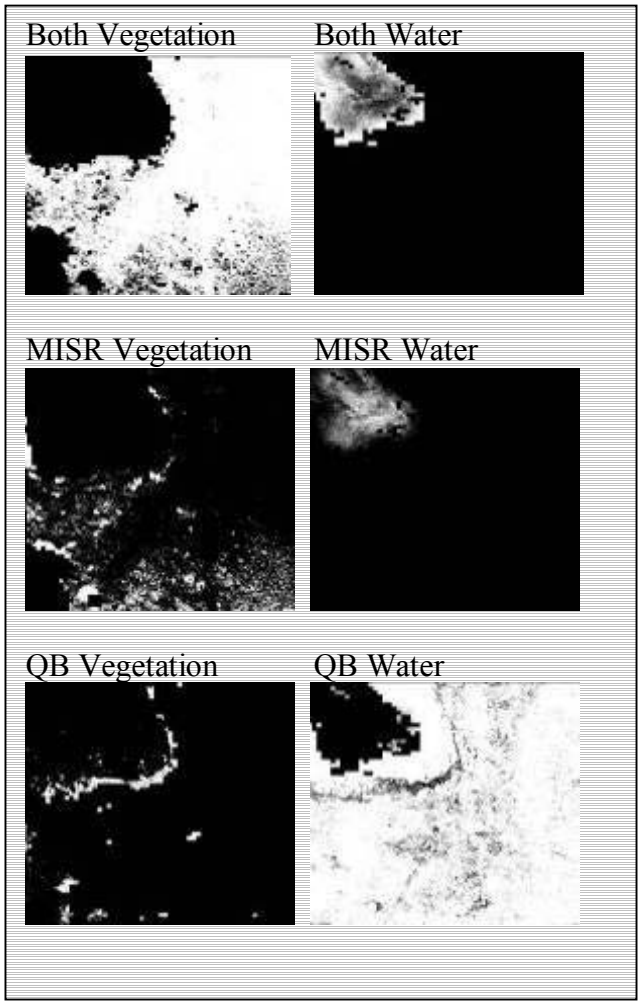

Figure 23. Comparison of multispectral + multiangular MISR and QuickBird estimates of water and vegetation for 2002. White pixels are where specified conditions were met. (20%-100% fraction coverage) – MISR resized to QuickBird

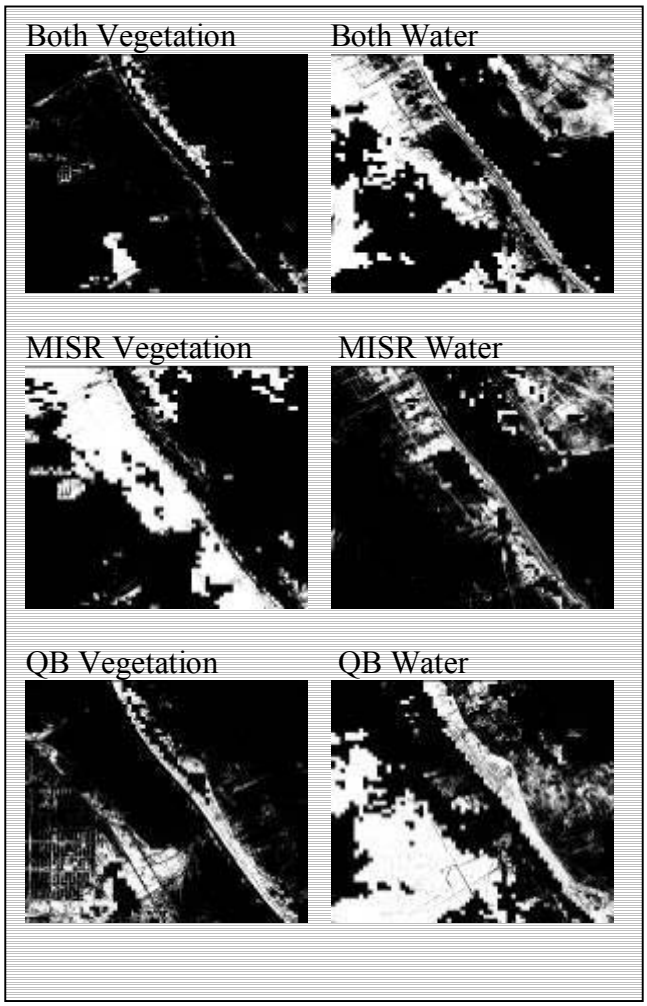

Figure 24. Comparison of multispectral + multiangular MISR and QuickBird estimates of water and vegetation for 2005. White pixels are where specified conditions were met. (20%-100% fraction coverage) – MISR resized to QuickBird

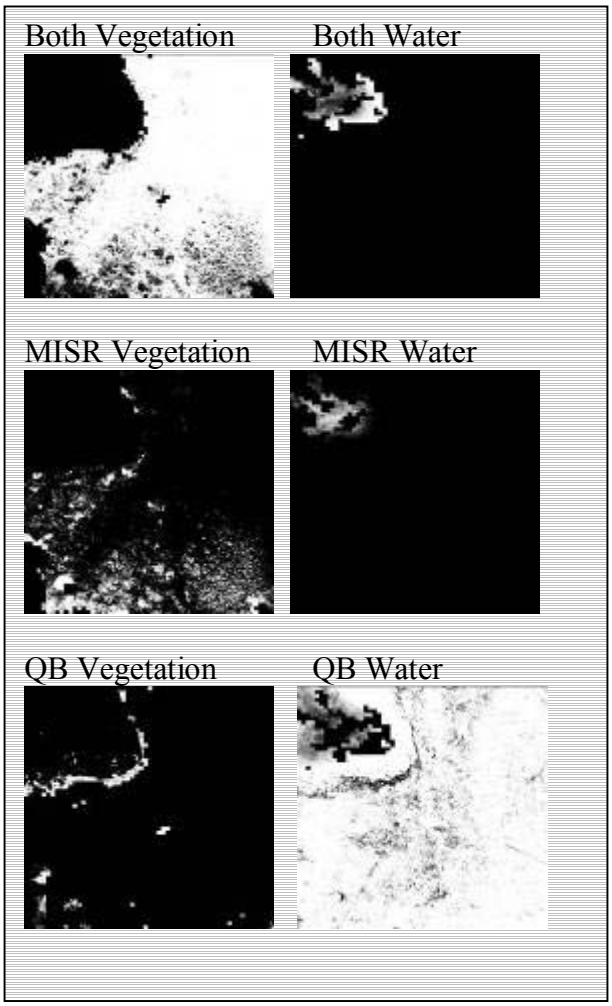

Figure 25. Comparison of multispectral MISR and QuickBird estimates of water and vegetation for 2002. White pixels are where specified conditions were met. (20%-100% fraction coverage) – MISR resized to QuickBird

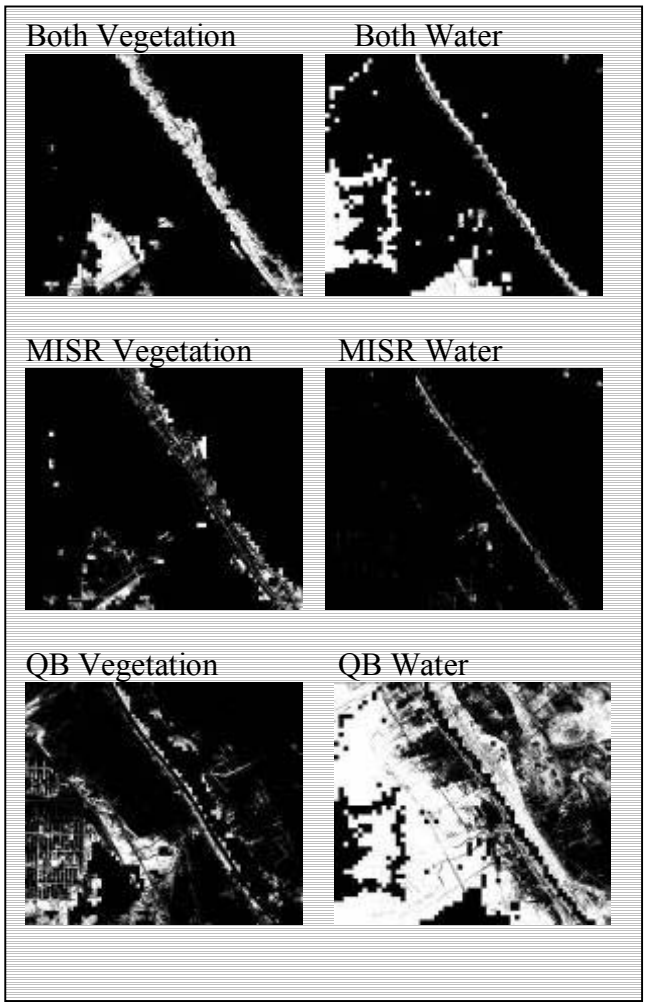

Figure 26. Comparison of multispectral MISR and QuickBird estimates of water and vegetation for 2005. White pixels are where specified conditions were met. (20%-100% fraction coverage) – MISR resized to QuickBird

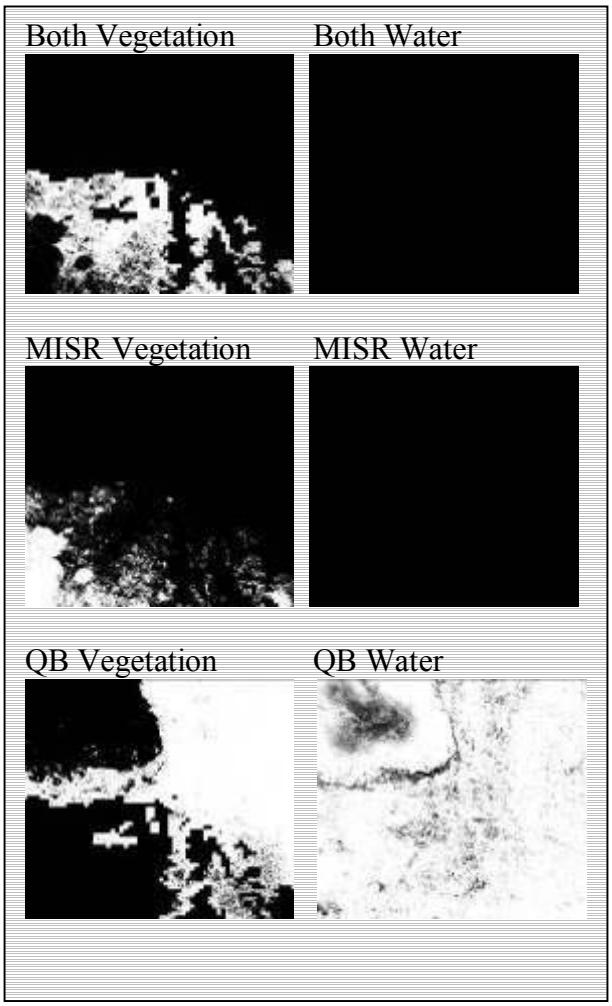

Figure 27. Comparison of multiangular MISR and QuickBird estimates of water and vegetation for 2002. White pixels are where specified conditions were met. (20%-100% fraction coverage) – MISR resized to QuickBird

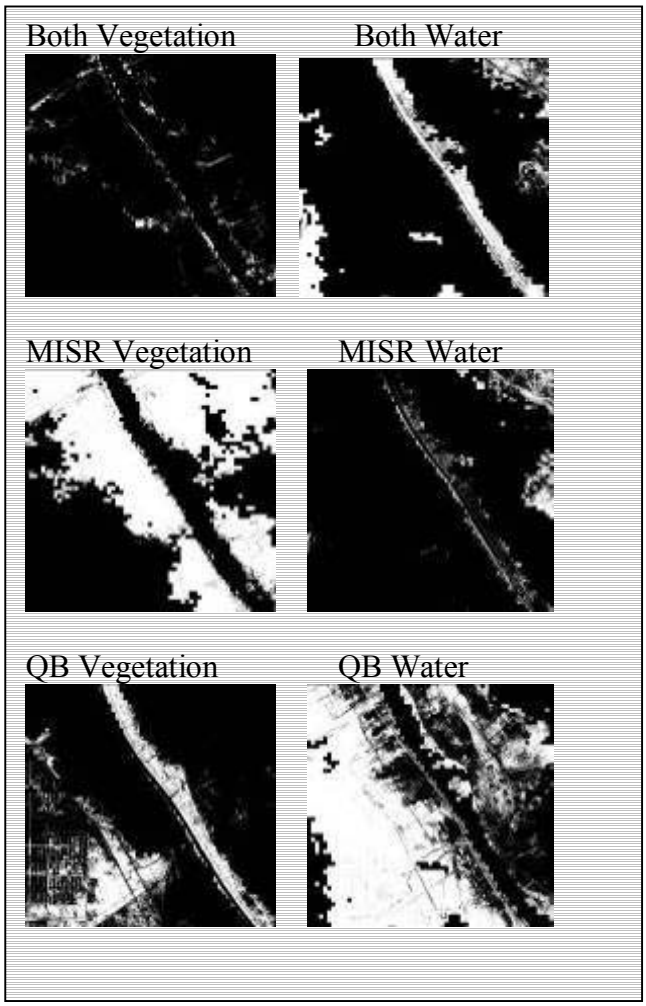

Figure 28. Comparison of multiangular MISR and QuickBird estimates of water and vegetation for 2005. White pixels are where specified conditions were met. (20%-100% fraction coverage) – MISR resized to QuickBird

Table 12. Image comparison of QuickBird and MISR (multispectral + multiangular, multispectral and multiangle) for 20% vegetation or water fraction. (MISR resized to QuickBird)

2002						
	Multiangular + Multispectral (km^2)	Percent (%) of Total Area	Multispectral area (km^2)	Percent (%) of Total Area	Multiangular (km^2)	Percent (%) of Total Area
Both Veg	168	57	188	64	59	20
Both Water	18	6	8	3	0	0
MISR Veg	21	7	25	8	32	11
MISR Water	9	3	4	1	0	0
QuickBird Veg	7	2	7	2	140	47
QuickBird Water	218	74	242	82	269	91
2005						
Both Veg	14	6	24	10	6	2
Both Water	88	37	28	12	39	16
MISR Veg	76	32	10	4	132	55
MISR Water	37	15	3	1	14	6
QuickBird Veg	42	17	27	11	49	20
QuickBird Water	99	41	128	53	148	61

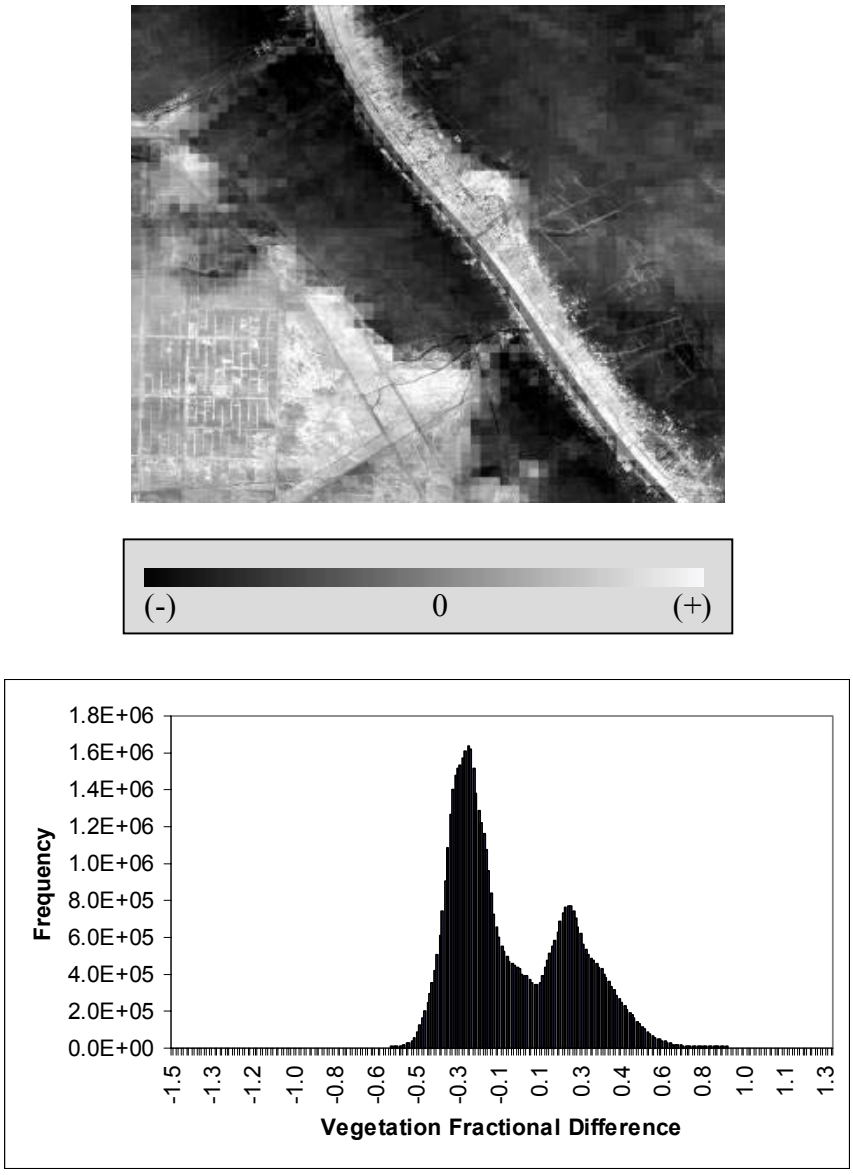

Figure 29. Vegetation fractional difference image for 2005 MISR multiangular subtracted from QuickBird (left). The histogram illustrating the bimodal distribution of image differences is on the right.

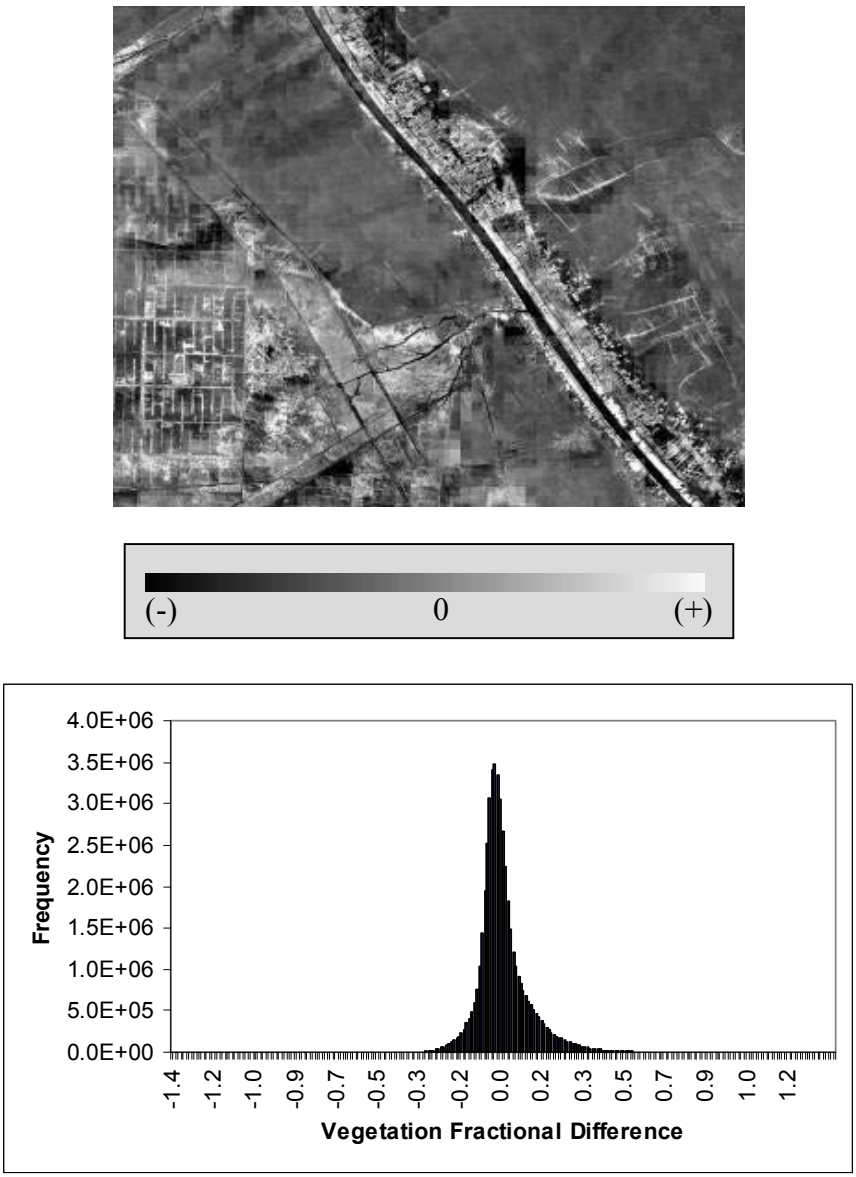

Figure 30. Vegetation fractional difference for 2005 MISR multispectral subtracted from QuickBird (left). The histogram illustrating the Gaussian distribution of image differences is on the right.

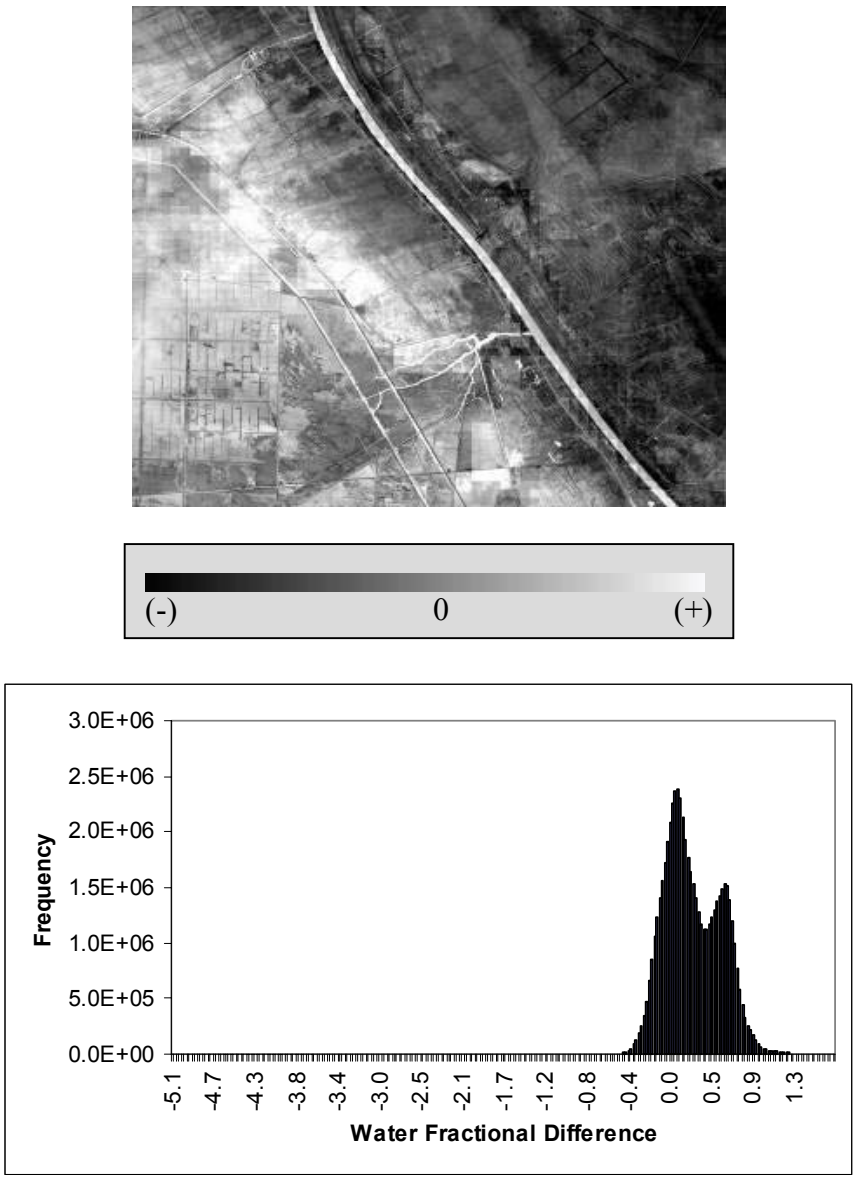

Figure 31. Water fractional difference for 2005 MISR multiangular subtracted from QuickBird (left). The histogram illustrating the bimodal distribution of image differences is on the right.

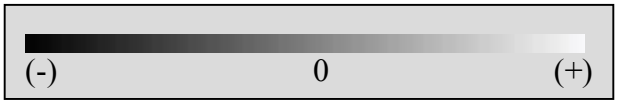

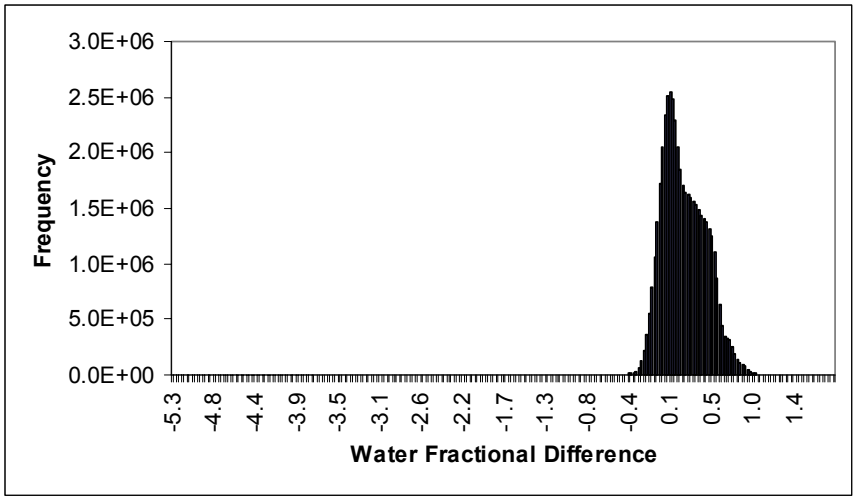

Figure 32. Water fractional difference for 2005 MISR multispectral subtracted from QuickBird (left). The histogram illustrating the positively skewed distribution of image differences is on the right.

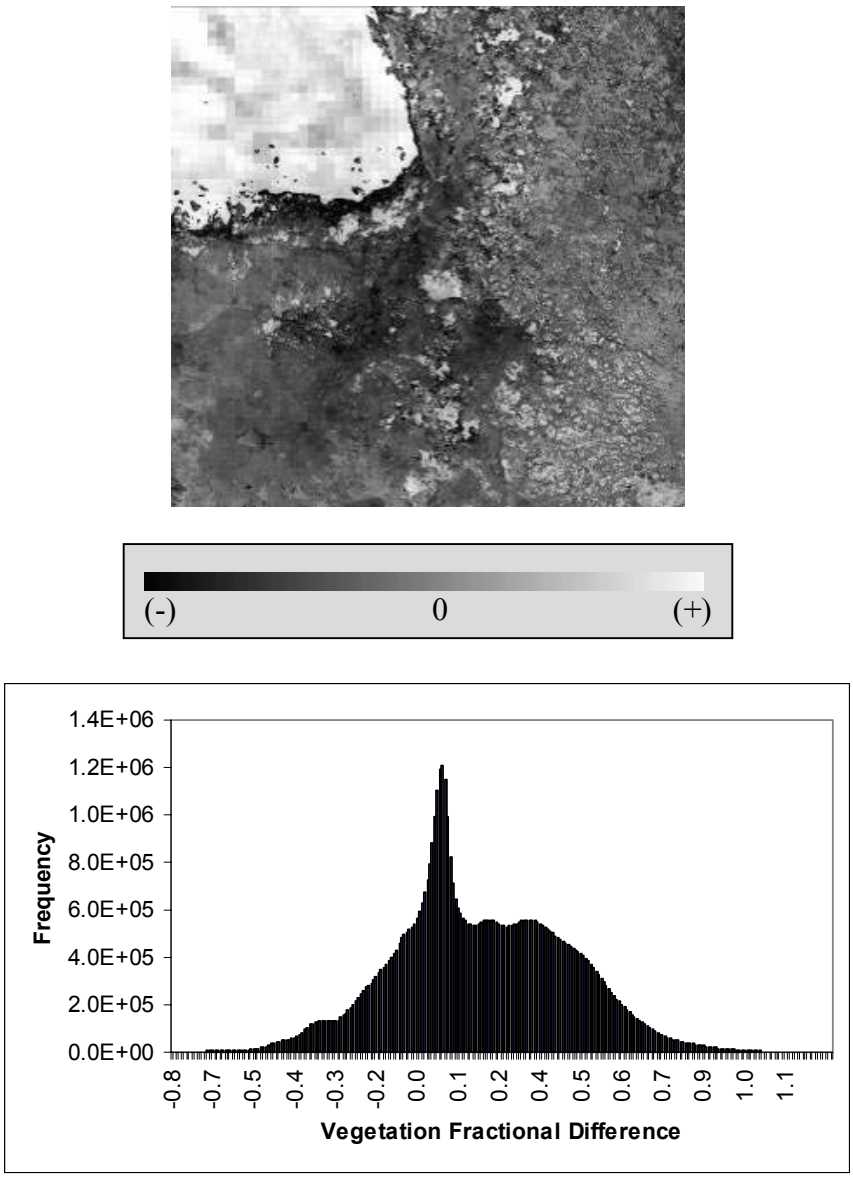

Figure 33. Vegetation fractional difference for 2002 MISR multiangular subtracted from QuickBird (left). The histogram illustrating highly kurtotic distribution of image differences is on the right.

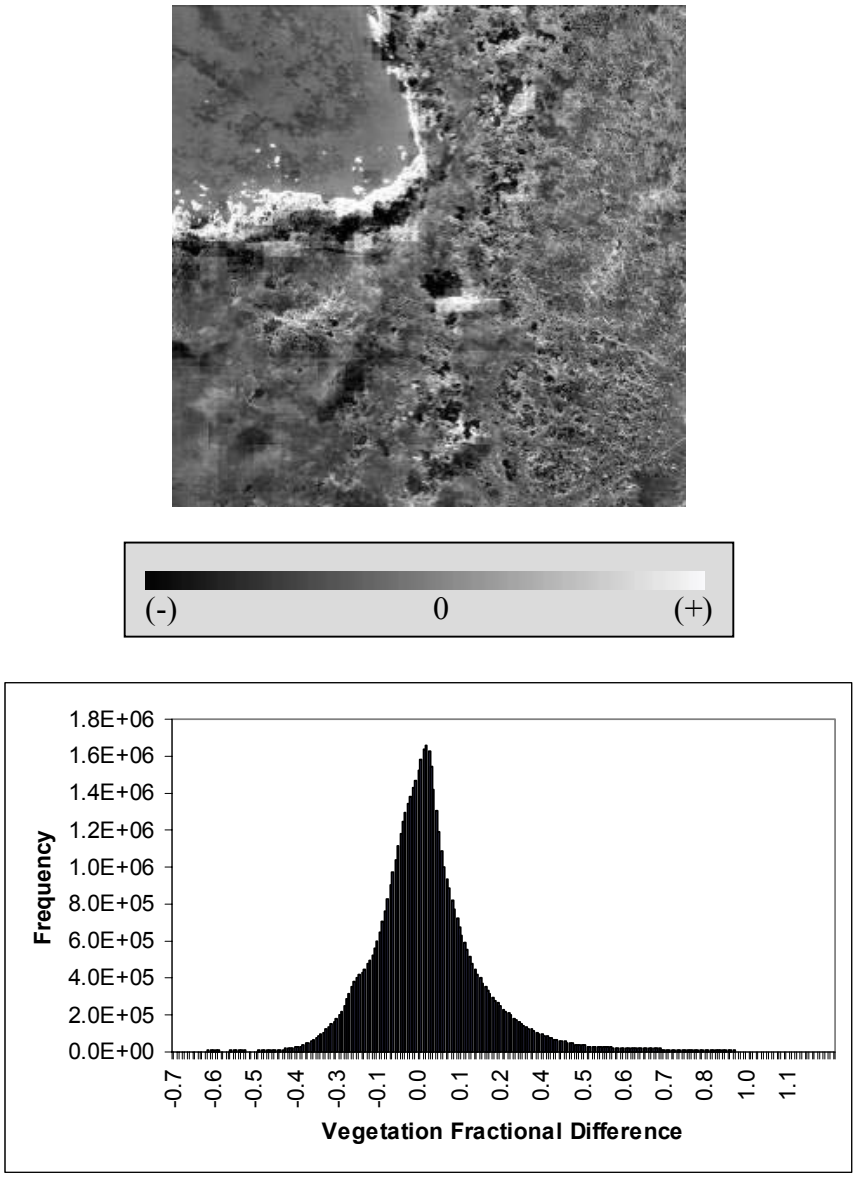

Figure 34. Vegetation fractional difference for 2002 MISR multispectral subtracted from QuickBird (left). The histogram illustrating the Gaussian distribution of image differences is on the right.

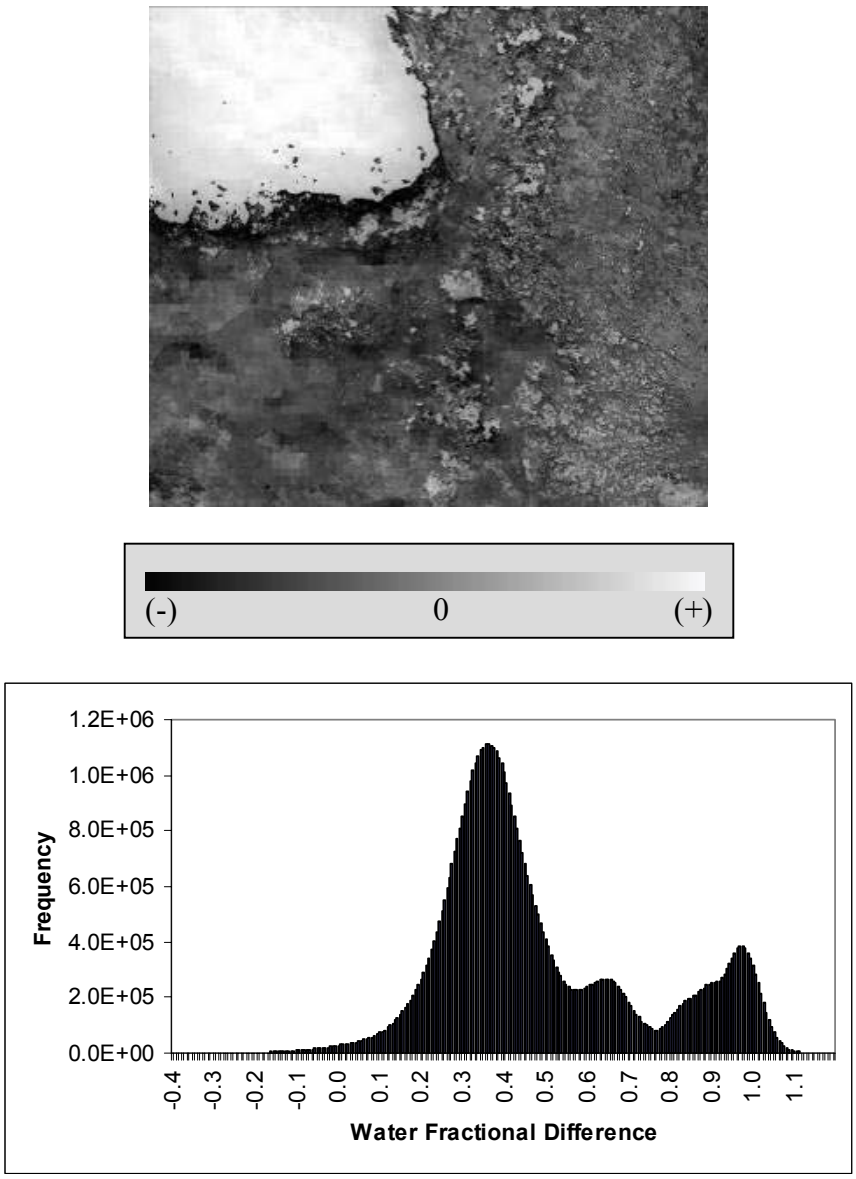

Figure 35. Water fractional difference for 2002 MISR multiangular subtracted from QuickBird (left). The histogram illustrating the trimodal distribution of image differences is on the right.

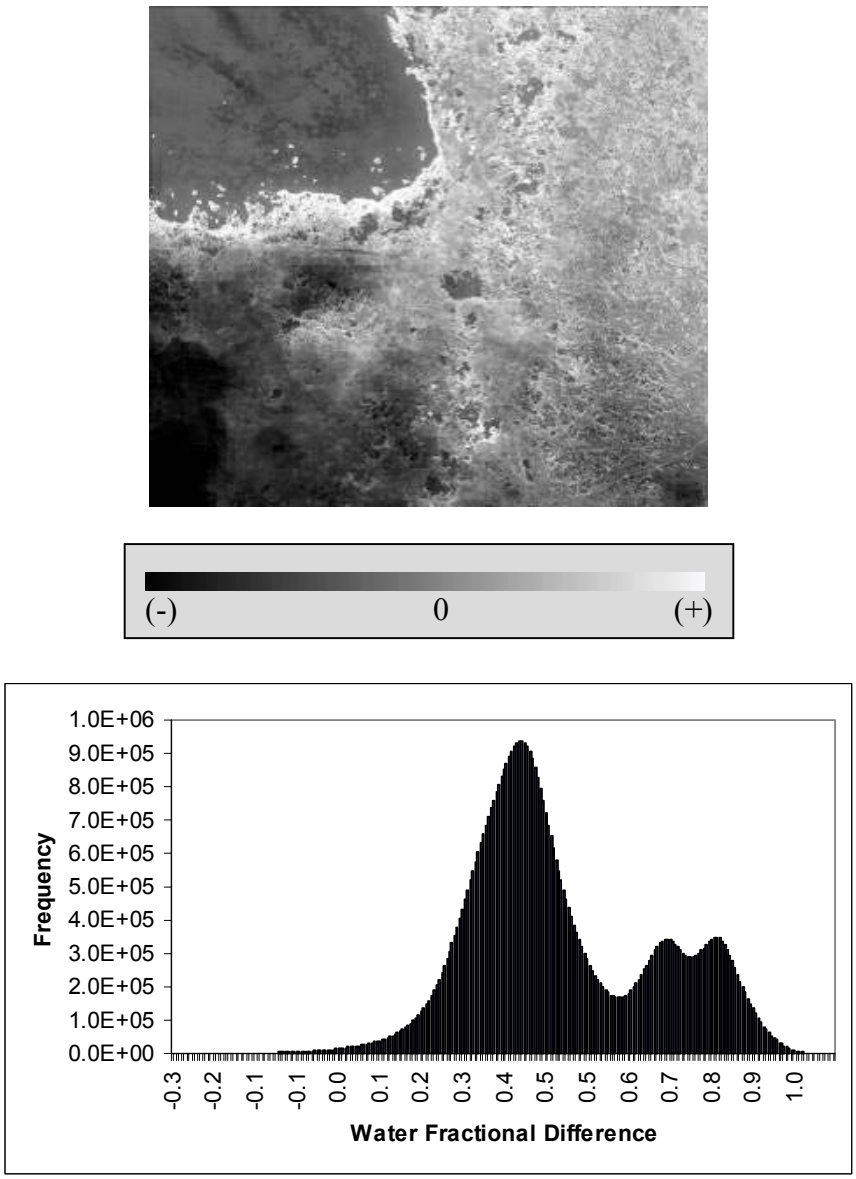

Figure 36. Water fractional difference for 2002 MISR multispectral subtracted from QuickBird (left). The histogram illustrating a trimodal distribution of image differences is on the right.

Error Analysis

Due to armed conflicts in the region ground truth data were unavailable. In lieu of ground data, this study relied on high spatial resolution QuickBird imagery for assessment of results. Each MISR 275-m pixel is roughly equivalent to about 18,906 QuickBird pixels. Because of these differences, the high-spatial resolution QuickBird is able to identify certain features that are not detectable in the coarser MISR imagery.

Image data were acquired at approximately the same date for each of the six years of the study. However, phenological differences will influence the results as will interannual variability of climate. Both papyrus and phragmites have been shown to have relatively high growth rates (Jones and Murthuri, 1985; Chambers et al., 1999). The variability in their growth rates and slight differences in the time of image acquisition may lead to inaccuracies in estimates of vegetation cover.

A related potential error can be attributed to the use of only six images. This study examined six MISR images from 2000 through 2005 that were acquired during the period following the traditional wet-seasons. However, due to the use of only one image a year, the region's variability in interseasonal hydrologic variables was not captured. When combined with the knowledge of key plant's highly variable growth rates, more images may be required and could possibly provide different results.

Because linear spectral unmixing results are highly dependent on the selected endmembers, correct endmember selection is vital. Endmember selection is also limited to the number of bands that are available. For example, when selecting

endmembers for the multispectral subset only four endmembers could be selected (the number of bands available). So, if there were five-distinct endmembers the unmixing model would only use four, thus influencing the results. Also, the spectral linear unmixing model fails to take into account non-linear mixing effects between materials.

Conclusion

This study compared three different aspects of the MISR multiangular data: a four band spectral subset, a nine-band angular subset and a combination of multispectral and multiangular data. Differences and similarities of each subset were then assessed with high spatial resolution QuickBird imagery. Results show that vegetation mapping with each subset of the MISR imagery had advantages and disadvantages. While each approach overestimated vegetation by some degree, all were able to identify large areas of vegetation that were confirmed by the QuickBird imagery.

Water, on the other hand, was consistently underestimated by all combinations of the MISR data. The QuickBird image identified a much larger area that was considered to have greater than 20% fractional coverage of water. The MISR images mapped fewer pixels as water and in a number of cases, when water was mapped in both MISR and QuickBird pixels, the MISR image water fraction was below the 20% threshold used to define a pixel as water. This suggests that when comparing two images of vastly different spatial resolutions, different thresholds might need to be considered.

When examining the spatial characteristics of each image, the spectral and angular signatures of each followed known patterns of reflectance as illustrated in previous studies of vegetation and water. Based on there results it might be reasonable to say the discrepancies in QuickBird and MISR are not significant and

that the MISR images are detecting traces of vegetation and water where the QuickBird images were unable to, thus validating the benefits of using multiangular data.

Additionally, when examining the results from the 2002 pixel-by-pixel comparisons we can see that the multispectral + multiangular image was able to accurately map 96% of the vegetation and 8% of the water, as identified by QuickBird. The multispectral subset also accurately identified 96% of the vegetation, but only 3% of the water. Lastly the multiangular subset was able to correctly identify 30% of the vegetation but 0% of the water. When looking at the 2005 comparisons the multispectral + multiangular image correctly identifies 25% of the vegetation and 47% of the water. The multispectral subset identifies 42% of the vegetation but only 18% of the water while the multiangular subset identifies 11% of the vegetation and 21% of the water.

When examining the 2002 and the 2005 comparisons we see that the multispectral + multiangular images consistently identified more areas of water than the multispectral or multiangular subset images. In 2002 both the multispectral + multiangular and the multispectral subset were able to accurately identify the largest percentage of vegetation. However, in 2005 vegetation is more accurately identified when using just the multispectral subset. Based on the results of these comparisons, we see that MISR multispectral + multiangular images are able to identify a higher percentage of water, as identified by QuickBird, than just the multispectral or

multiangular subsets. In order to make a similar statement about vegetation, more studies are required.

This study used six images (one per year), from a period that followed historical wet-seasons. With the addition of more MISR images, MISR's ability to identify vegetation in wetlands would be validated. More images would also allow for differences in interseasonal and interannual differences to be assessed. The assessment of these differences would provide a more accurate description and understanding of the changes that this ecosystem has undergone.

This study only acquired two high spatial resolution QuickBird images to be used in the pixel-by-pixel comparisons. Both of the images were acquired around the same time of year, but three years apart and in different locations. In order to improve accuracy, images of the same location should be acquired for each year.

Because of QuickBird's high spatial resolution the sensor has a small IFOV (instantaneous field of view), which reduces the amount of energy that can be detected on the surface. MISR on the other hand has a much coarser resolution and is limited in its ability to identify subtle differences in an image. An optimal set of sensors would provide images that were acquired seasonally, at 15-30 meter resolution and a radiometric resolution of at least 8-bit. With a larger IFOV the ability to detect small changes in energy is increased. Additionally a coarser spatial resolution would improve radiometric and spectral resolutions. Therefore a intermediate resolution between the high spatial resolution QuickBird and the low resolution MISR is recommended.

Building on the success of previous multispectral and multiangular studies, this study was able to generate a six-year record of change in vegetation density and water inundation patterns for the Mesopotamian Marshlands. Results validate the effectiveness of multispectral + multiangular MISR to detect water inundation in a recovering wetland. The effectiveness to detect vegetation densities is very encouraging but still requires some research. Additionally the spectral linear unmixing model has been implemented so that sub-pixel estimates of vegetation coverage and water inundation can be determined. The mapping methods tested in this study, the first of its kind, all show increases in vegetation densities and water inundation in this important ecosystem. With the addition of more images that capture seasonal differences and images that validate those results, important, accurate information regarding vegetation re-growth and the emergence of water in a recovering wetland could be obtained. Based on the results of this study, areas that appear to be recovering quite well and others areas that are not can clearly be identified. These maps can help provide the basis for future restoration and monitoring efforts.

References

Adams, J., Smith, M., and P. Johnson. 1986. Spectral mixture modeling – A new analysis of rock and soil types at the Viking Lander 1 site. *Journal of Geophysical Research*, 91: 8098-8112.

Al-Saboonchi, A., Mohamed, A., and N.Barak. 1982. A study of phytoplankton in the Garma marshes, Iraq. *Iraqi Journal of Marine Science*, 1982. 1(1): 67-78.

Alwash, S. 2003. Senior Project Advisor, The Eden Again Project. http://www.edenagain.org/marshlandinfo.html. Last Date Accessed, 02 November 2006.

Asner, G., and K. Heidebrecht. 2002. Spectral unmixing of vegetation, soil and dry carbon cover in arid regions: comparing multispectral and hyperspectral observations. *International Journal of Remote Sensing*, 23 (19): 3939-3958.

Asner, G., Wessman, C., and J. Privette. 1997. Unmixing the Directional Reflectances of AVHRR Sub-Pixel Landcovers. *IEEE Transactions on Geosciences and Remote Sensing,* 35 (4): 868-878.

Banister, K., Backiel, T., and J. Bishop. 1994. The present state and likely future of the fishes of the Tigris-Euphrates Basin. Unpublished report. Wetland Ecosystems Research Group, University of Exeter.

Boardman, J., and F. Kruse. 1994. Automated spectral analysis: a geological example using ACRIS data, north Grapevine Mountains, Nevada. *Proceedings, ERIM Tenth Thematic Conference on Geologic Remote Sensing*, Environmental Research Institute of Michigan, Ann Arbor, MI: l-407-l-418.

Chambers, R., Meyerson, L., and K. Saltonstall. 1999. Expansion of Phragmites australis into tidal wetlands of North America. *Aquatic Botany*, 64: 261-273.

Chang, C., and H. Ren. 2000. An experiment-based quantitative and comparative analysis of target detection and image classification algorithms for hyspectral imagery. *IEEE Transactions on Geocience and Remote Sensing*, 38 (2): 1044-1063.

Chen, C., Hepner, G., and R. Forster. 2003. Fusion of hyspectral and radar data using the HIS transformation to enhance urban surface features. *ISPRS Journal of Photogrammetry and Remote Sensing*, 58: 19-30.

Chopping, M., Rango., Havstad, K., Schiebe, F., Richie, J., Schmugge, T., French, A., Su, L., McKee, L., and M. Davis. 2003. Canopy attributes of desert grassland and transition communities derived from multiangular airborne imagery. *Remote Sensing of the Environment,* 85; 339-354.

Chopping, M., Su, L., Lailberte, A., Rango, A., Peters, D., and N Kollikkathara. 2006. Mapping shrub abundances in desert grasslands using geometric-optical modeling and multi-angle remote sensing with CHRIS/Proba. *Remote Sensing of the Environment*, 104 (1): 62-73.

Colombo, R., Bellingeri, D., Fasolini, D., and C. Marino. 2003. Retrieval of leaf area index in different vegetation types using high resolution satellite data. *Remote Sensing of Environement*, 86: 120-131.

Diner, D., Beckert, J., Reilly, T., Bruegge, C., Conel, J., Kahn, R., Martonchik, J., Ackerman, T., Davies, R., Gerstl, S., Gordon, H., Muler, J-P., Myneni, R., Sellers, P., Pinty, B., Verstraete, M. 1998. Multi-angle Imaging SpectroRadiometer (MISR) Instrument Description and Experiment Overview. *IEEE Transaction on Geoscience and Remote Sensing*, 36(4): 1072-1087.

Embassy of the Republic of Turkey. Washington D.C. USA. http://www.turkishembassy.org/index.php?option=com_content&task=view&id=47&Itemid=67. Last Date Accessed, 02 November 2006.

Green, A., Berman, M., Switzer, P., and M. Craig. 1988. A transformation for ordering multispectral data in terms of image quality with implication for noise removal. *IEEE Transactions on Geoscience and Remote Sensing*, 26 (1): 65-74.

Gruen, G. 2002. Turkish Waters: Source of regional conflict or catalyst for peace? *Water, Air, and Soil Pollution*, 123: 565-579.

Hapke, B. 1993. *Theory of Reflectance and Emittance Spectroscopy*. Cambridge Univ. Press, Cambridge, UK, 469pp.

Hess, L., Melack, J., Novo, E., Barbosa, C., and M. Gastil. 2003. Dual-season mapping of wetland inundation and vegetation for central Amazon basin. *Remote Sensing of the Environment*, 87: 404-428.

Hinton, G., and B. Maulood. 1980. Some diatoms from brackish water habitats in southern Iraq. *Nova-Hedwigia,* 33 (1-2): 475-486.

Hinton, G. and B Maulood. 1982. Contributions to the Algal Flora of Iraq - the Non-Diatom Flora of the Southern Marshes. *Nova Hedwigia* 36(1): 49-64.

Jensen, J. 2005. Introductory Digital Image Processing: A Remote Sensing Perspective, 3rd Edition. Pearson Prentice Hall, Pearson Education, Inc. Upper Saddle River, NJ 07458. pg 454.

Johnson, L., Roczen, D., Youkhana, S., Nemani, R., and D. Bosch. 2003. Mapping vineyard leaf area with multispectral satellite imagery. *Computers and Electronics in Agriculture*, 38: 33-44.

Jones, M. and F. Muthuri. 1985. The Canopy Structure and Microclimate of Papyrus (Cyperus Papyrus) Swamps. *Journal of Ecology*, 73: 481-491.

Jordan, C.F. 1969. Derivation of leaf area index from quality measurements of light on the forest floor. *Ecology*, 50: 663-666.

Kliot, N. 1994. Water Resources and Conflict in the Middle East. Routledge, London and New York.

Maltby, E. 1994. An Environmental and Ecological Study of the Marshlands of Mesopotamia. Draft Consultative Bulletin. Wetland Ecosystems Research Group. AMAR Appeal Trust, London.

Mann, A. 2003. The Southeastern Anatolia Project (GAP) and Archaeology. *The Worlds Water*: The Biennial Report on Freshwater Resources 2002-2003, vol (3): 181-193. Island Press, 1718 Connecticut Avenue, NW Suite 300 Washington DC 20009.

Mertes, L. 1997. Documentation and significance of the perirheic zone on inundated floodplains. *Water Resources Research*, 33: 1749-1762.

NASA Langley Research Center. 2006. Last Date Accessed, 02 November 2006. http://eosweb.larc.nasa.gov/PRODOCS/misr/FAQ.html

Nolin, A. 2004. Towards retrieval of forest cover density over snow from Multi-angle Imaging SpectroRadiometer (MISR). *Hydrological Processes*, 18: 3623-3636.

Partow, H. 2001. The Mesopotamian Marshlands: Demise of an Ecosystem. Early Warning and Assessment Technical Report UNEP/DEWA/TR.01-3, 58pp, United Nations Environmental Program, Washington D.C.

Petrou, M., and P., Foschi. 1999. Confidence in Linear Spectral Unmixing of Single Pixels. *IEEE Transactions on Geosciences and Remote Sensing,* 37 (1): 624-644.

Pinty, B., Widlowski, J-L., Gobron, N., Verstraete, and D. Diner. 2002. Uniqueness of Multiangular Measurements -- Part I: An Indicator of Subpixel Surface Heterogeneity from MISR. *IEEE Transactions on Geosciences and Remote Sensing,* 40 (7): 1560-1573.

Republic of Turkey Prime Ministry Southeastern Anatolia Project Regional Development Administration. 2005. http://www.gap.gov.tr/gapeng.html. Last date accessed 02 November 2006.

Richardson, C., Reiss, P., Hussain, N., Alwash, A., and D. Pool. 2005. The Restoration Potential of the Mesopotamian Marshes of Iraq. *Science,* 307 (5713): 1307-1311.

Richardson, A. J. and Wiegand, C. L. 1977. Distinguishing vegetation from soil background information, *Photogrammetric Engineering and Remote Sensing*, 43: 1541-1552.

Rogers A., and M. Kearney. 2003. Reducing signature variability in unmixing coastal marsh Thematic Mapper scenes using indices. *International Journal of Remote Sensing*, 25 (12): 2317-2335.

Rouse, J.W., R.H.Haas, J.A.Schell, and D.W.Deering, 1973: Monitoring vegetation systems in the great plains with ERTS, Third ERTS Symposium, NASA SP-351 I: 309-317.

Schmid, T., Koch, M., Gumuzzio, J., and P. Mather. 2004. A spectral library for a semi-arid wetland and its application to studies of wetland degradation using hyspectral and multispectral data. *International Journal of Remote Sensing*, 25 (13): 2485-2496.

Scott, D., and M. Evans. 1994. Wildlife of the Mesopotamian Marshlands. Report prepared for Wetlands Ecosystem Research Group, University of Exeter, U.K.

Scott, D. 1995. A Directory of Wetlands in the Middle East. IUCN, Gland, Switzerland and IWRB, Slimbridge, UK.

Smith, L. 1998. Satellite remote sensing of river inundation area, stage, and discharge: a review. *Hydrological Processes,* 11(10): 1427–1439.

Thesiger, W. 1957. Marsh Dweller of Southern Iraq. *National Geographic*, CXIII: 204-239.

Vanderbilt, V., Perry, G., Livingston, G., Ustin, S., Barrios, M., Breon, F-M., Leroy, M., Balois, J-Y., Morrissey, L., Shewchul, S., Stearn, J., Zedler, S., Syder, J., Bouffies-Cloche, S., and M. Herman. 2002. Inundation Discriminated Using Sun Glint. *IEEE Transactions on Geoscience and Remote Sensing,* 40(6): 1279-1287.

Zhu, H. 2005. Linear spectral unmixing assisted by probability guided and minimum residual exhaustive search for subpixel classification. *International Journal of Remote Sensing*, 26 (24): 5585-5601.